2018

Development of a Functional In Vitro 3D Model of the Peripheral Nerve

Wesley Anderson
University of Central Florida

DEVELOPMENT OF A FUNCTIONAL IN VITRO 3D MODEL OF THE PERIPHERAL NERVE

by

WESLEY ALLEN ANDERSON
B.S. UNIVERSITY OF CENTRAL FLORIDA, 2011
M.S. UNIVERSITY OF CENTRAL FLORIDA, 2013

A dissertation submitted in partial fulfillment of the requirements
for the degree of Doctor of Philosophy
in the Burnett School of Biomedical Sciences
in the College of Medicine
at the University of Central Florida
Orlando, Florida

Summer Term
2018

Major Professor: Stephen Lambert

ABSTRACT

Peripheral neuropathies, affect approximately 20 million people in the United States and are often a complication of conditions such as diabetes that can result in amputation of affected areas such as the feet and toes. In vitro methodologies to facilitate the understanding and treatment of these disorders often lack the cellular and functional complexity required to accurately model peripheral neuropathies. In particular, they are often 2-D and functional readouts, such as electrical activity, are limited to cell bodies thereby limiting the understanding of axonopathy which often characterizes these disorders.

We have developed a functional 3-D model of peripheral nerves using a capillary alginate gel (Capgel™), as a scaffold. We hypothesize that: 1) The unique microcapillary structure of Capgel™ allows for the modeling of the 3-D microstructure of the peripheral nerve, and 2) That axon bundling in the capillary allows for the detection of axonal electrical activity.

In our initial studies, we demonstrate that culturing embryonic dorsal root ganglia (DRG) within the Capgel™ environment allows for the separation of cell bodies from axons and recreates many of the features of an in vivo peripheral nerve fascicle including myelinated axons and the formation of a rudimentary perineurium. To develop functionality for this model we have integrated the DRG Capgel™ culture with a microelectrode array to examine spontaneous activity in axon bundles, which we find demonstrates superiority to other widely used 2-D models of the same tissue. Furthermore, by analyzing the activity on individual electrodes, we were able to record action potentials from multiple axons within the same bundle indicating a functional complexity comparable to that observed in fascicles in vivo. This 3D model of the

peripheral nerve can be used to study the functional complexities of peripheral neuropathies and nerve regeneration as well as being utilized in the development of novel therapeutics.

ACKNOWLEDGMENTS

Thank you, Steve for the best graduate school experience I could hope for. I appreciate all our discussions; personal and professional. Thanks for keeping me interested in my passion of science and allowing me to do the experiments I wanted to do, wherever they led me. Allowing me to independently manage my own projects and undergraduate students has provided me with priceless experience, which will help me in my future career endeavors.

Thank you to my committee members Dr. Cristina Fernandez-Valle, Dr. James Hickman, Dr. Alvaro Estevez, and Dr. Bradley Willenberg for always supporting me and helping me look at problems from different perspectives. Your constructive criticism has been of great help for me to understand all aspects on the problems I encounter and I have always enjoyed our meetings. I am humbled to be fortunate enough to have received advice from so many great scientists.

To my parents, for always supporting my dreams and helping me out with whatever I needed, thank you. Your constant encouragement has been greatly appreciated. Thank you, Alisha for your constant support and dealing with the ups and downs I've gone through. I'm lucky to have met you and can't wait to see what lies ahead for us. Thank you to all of my friends and family for your unwavering support.

Thank you to everyone I've worked with in the lab. Dale, you have always been right at my side with all our experiments and shared in all the excitement of what our lab has produced. You made coming into lab a joy and I truly appreciate all your help. Thanks again Brad, for working with me on Capgel™ and making this all possible. Alex, thanks for all your

contributions toward this work and your insightful inputs. Alicia your input on my projects and work with the cryostat was greatly appreciated. Thank you, Rachel, Peter, Paige, Anita, Christina, Jacob for your help in the lab.

Special thanks to Dr. Hickman's lab group for starting my tissue engineering training. Thank you, Dr. Hickman for seeing my passion for tissue engineering and immediately bringing me into the lab. Your mentorship and advice were greatly appreciated and I wouldn't be where I am today without it. Thank you, Chris Long and Craig Finch for taking me under your project and personally mentoring me and for teaching me methods for integrating engineering techniques with biology. Thank you Chris McAleer, Alec Smith and Bonnie Berry, Xiufang Guo, Maria Stancescu, and Mark Schnepper for teaching me essential cell culture skills and your useful career advice, which I still use to this day. In addition I'd like to thank the members of the Estevez, Fernandez-Valle, and Willenberg labs for their advice and help throughout the years. Nick and Marga helped me get my start with culturing cells for the lab, which I am extremely grateful for. Nick, you were always available to help me with whatever I needed from microscopes to cell culture advice, your expertise was appreciated. Thank you, Cassandra with all your help with motor neuron cultures and sharing your skills with me.

Thank you to the Burnett School of Biomedical Sciences department for working with me and helping me when I needed it. Thank you, Ryan Dickerson, the medical illustrator, for your contribution as well as the vivarium staff.

TABLE OF CONTENTS

LIST OF FIGURES

LIST OF ACRONYMS

Capgel™	Capillary Alginate Gel
DRG	Dorsal Root Ganglion
MBP	Myelin Basic Protein
MEA	Microelectrode Array
NGC	Nerve Guidance Conduit
NGF	Nerve Growth Factor
NGS	Normal Goat Serum
OCT	Optimal Cutting Temperature Compound
PBS	Phosphate Buffered Saline
PFA	Paraformaldehyde
pNF	Phosphorylated Neurofilament
PORN	Poly-L-Ornithine
RT	Room Temperature
SCP	Schwann Cell Precursor
SEM	Standard Error Mean

CHAPTER ONE: INTRODUCTION

Nerve Fascicle Structure

The somatic peripheral nervous system is made up of the ventral and dorsal rootlets, merging into spinal nerves and further leading into the peripheral nerves and their branches (Stewart, 2003). These peripheral nerves are made up of a composition of the somatic motor and sensory nerves (shown in Figure 1) in addition to the autonomic nerves (Campbell et al., 2008). Motor nerves send signals from their connections in the spinal cord to their effector muscles, while sensory nerves bring information to the spinal cord.

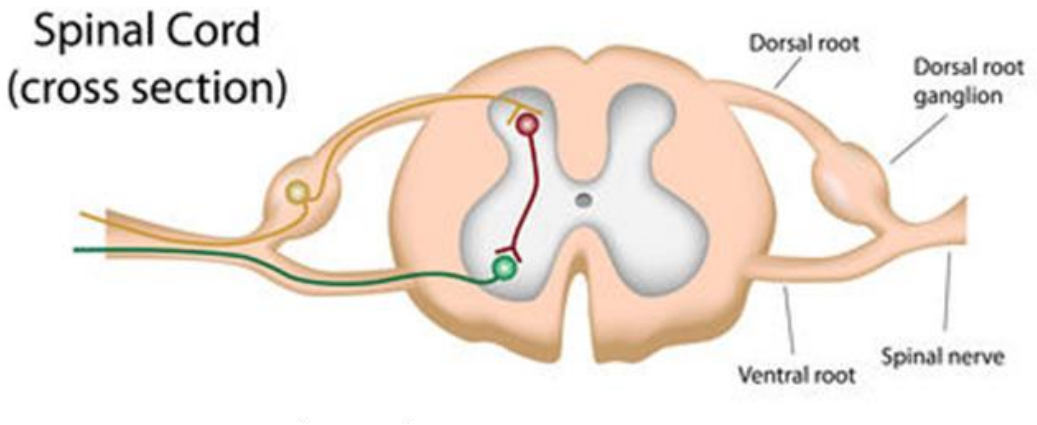

Figure 1 Cross section of spinal cord showing sensory and motor pathways.

When the cross-section of the peripheral nerve is analyzed (Konofaos et al., 2013) (Figure 2A, B) individual nerve fibers are bundled together in units called nerve fascicles. The nerve fascicle is an organized structure containing bundles of myelinated and non-myelinated axons. Figure 2B depicts an adult rat sciatic nerve fascicle with axons stained green (pNF) and

Schwann cell myelin in red (MBP). The perineurium can also be appreciated here as the flat cells lining the perimeter of the fascicle. Smaller nerves are made up of one nerve fascicle unit, while larger nerves are made up of multiple units. Many of the larger caliber axons are ensheathed by myelinating Schwann cells on a one-to-one basis, while the smaller axons are ensheathed by non-myelinating Schwann cells forming Remak bundles. Axons are embedded in the endoneurium, which is made of extracellular matrix made by endoneurial fibroblasts and Schwann cells. These units are then bundled and surrounded by the perineurium ultimately forming a nerve fascicle. The size and number of nerve fascicles can vary widely between nerves and the location, related proximally or distally, toward the target innervations (Stewart, 2003). Finally, encapsulating multiple nerve fascicles and their accompanying blood supply is the epineurium, forming a protective sheath around the entire nerve.

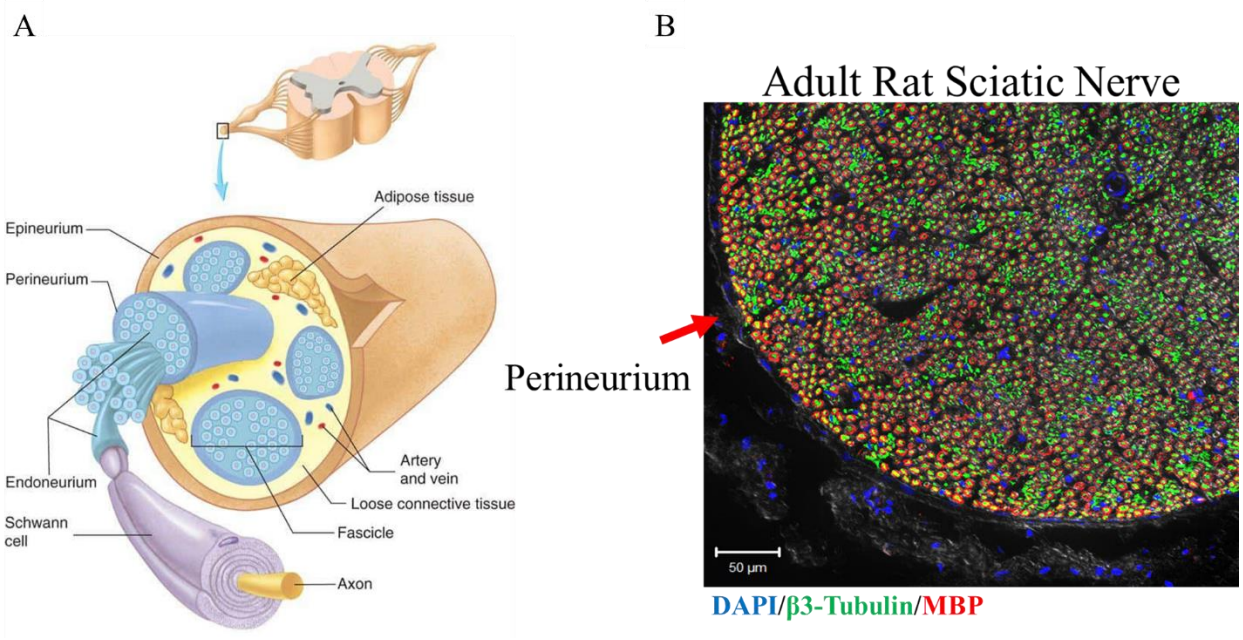

Figure 2 Peripheral nerve structural organization.

(A) Image shows the breakdown of peripheral nerve organization. (B) Image shows a cross section of an adult rat sciatic nerve demonstrating the different levels of nerve organization from Schwann cells myelinating (red) neuronal axons (green) bundled together with non-myelinated axons and blood vessels surround by the perineurium (arrow) to form the nerve fascicle. Scale bar in B is 50µm.

The perineurium plays a similar role to the CNS blood-brain barrier in that it forms a blood-nerve barrier, which is enriched in tight junctions. It is composed of several concentric layers of flat cells. This number of layers varies depending on multiple factors such as number of fascicles in a nerve and proximity to nerve endings, and can vary from one layer to up to 15 cell layers thick. Its main functions include maintaining the intrafascicular pressure and acting as a selective blood-nerve barrier for maintaining a precisely regulated microenvironment for the reliable neuronal activity (Kim et al., 2006) of axons and Schwann cells. Studies have also shown a protective immunological effect, as perineurial glia secrete surface complement regulators and inhibitors (Pina-Oviedo and Hidalgo, 2008). Perineurial glia interact with Schwann cells throughout development and are necessary for proper PNS development and health (Mirsky et al., 1999; Kucenas, 2015).

Nerve Development

Peripheral nerve development begins with neural crest cells migration from the neural tube through immature connective tissue around embryonic day 10-11 (e10-11) before the nerve has been formed (Jessen and Mirsky, 2005)(Figure 3A). These cells then generate Schwann cell precursor (SCPs), which tightly associate with bundles of axons (Jessen and Mirsky, 2005) as these early nerves migrate to their target innervation sites around e14-15 in the rat. SCPs provide

trophic support to sensory and motor neurons and are in involved in the regulation of perineurium development and nerve fasciculation (Garratt et al., 2000). At this stage in development, these structures are exclusively comprised of SCPs and tightly compact axon bundles and do not yet contain connective tissue or vascularization (Figure 3B). Once the developing nerves reach their targets, SCPs differentiate and give rise to the immature Schwann cells. There is also evidence showing a link of SCPs differentiating into fibroblasts found in the developing nerves (Joseph et al., 2004). Once the nerves form a structure more reminiscent of the adult nerve (e18-19) immature Schwann cells are found associated with axons and a developing perineurium forms defining the early nerve fascicle (Figure 3C). At this point, invading blood vessels as well as endoneurial fibroblasts are present.

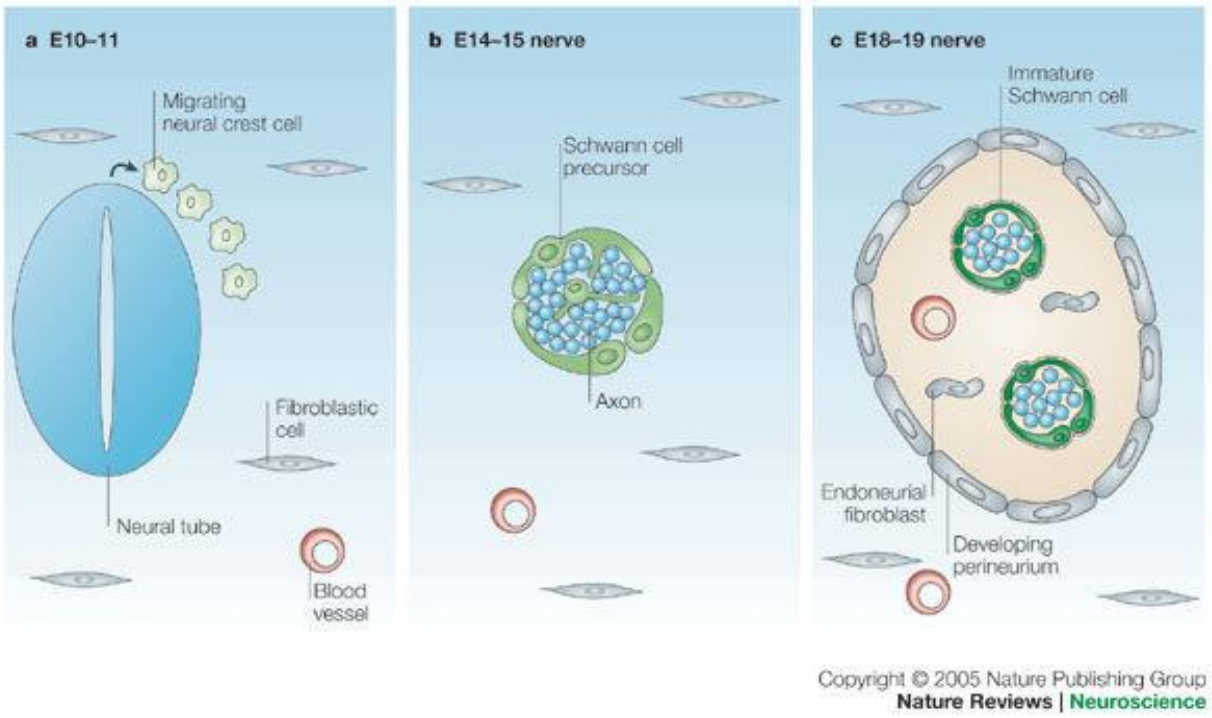

Figure 3 Cell and tissue organization at key stages of nerve development in rodents.

Clinical Relevance

20 million people in the United States suffer from peripheral neuropathies, resulting in 50,000 peripheral nerve repairs conducted annually (Lundborg, 2003). Nerve injuries account for $150 billion in annual healthcare costs in the US spent yearly (Taylor et al., 2008). These nerve injuries can stem from mechanical injuries, diabetes, and autoimmune diseases and have the potential to greatly lower the quality of life for patients. These symptoms include sensory and motor deficits, which can cause paralysis of the affected limbs and loss of sensation (Grinsell and Keating, 2014). While there can be some natural recovery for the less severe nerve injuries, most

require surgical intervention. The goal of peripheral nerve repair is the reinnervation of the target organs by sensory, motor, and autonomic axons and the guidance of these towards the distal nerve with minimal loss of nerve fibers (Brushart, 1991; Grinsell and Keating, 2014).

Current research into peripheral nerve repair highlights the autograft as the "gold standard," which can be used for bridging nerve sections up to 5cm. The autograft comes with the downfall of being removed from the patient and the accompanying issue of donor-site morbidity. Alternatively, work has been done with allografts, but this comes with the need of immunosuppressants. This has led to the need for bioengineered nerve guidance conduits, which do not suffer from either of these pitfalls. The goal for these devices is to act as a bridge between the proximal and distal nerve ends of the severed nerve, and allow for regeneration that leads to recovery of the normal function. By using these structures, there is hope that longer distances between the severed nerve pieces can lead to functional recovery. Some such devices are in use today for peripheral nerve repairs, but currently can only be used to bridge gaps up to 4cm (de Ruiter et al., 2009; Daly et al., 2011). Many of these FDA approved conduits are structurally simple tubes, which fail to mimic the microarchitecture of the normal nerve fascicle. Work done in developing the optimal conduits for peripheral nerve repair in addition to in vitro models that more accurately represent the in vivo peripheral nerve has led to the use of three-dimensional nerve models in vivo and in vitro.

Three-Dimensional Nerve Models

Two-dimensional cell culture models have been extensively used to study the nervous system and its functions in vitro (Trotter, 1993; Wood et al., 1990). Using DRGs or peripheral

nerves as the primary cell sources, work has been done using organotypic (Gatto et al, 2003) and dissociated cell culture models, which are commonly derived from the sciatic nerve (Windebank et al., 1985). While these models clearly have their uses, including reduced cost compared to animal studies, they lack the complex structural and functional features observed in a three-dimensional environment. These two-dimensional models lack key cell-to-cell and cell-to-ECM interactions that are conserved in vivo (Breslin and O'Driscoll, 2013).

Three-dimensional models are currently being used today to study the PNS (Breslin and O'Driscoll, 2013). Efforts to study the efficacy of nerve conduits for nerve regeneration has led to three-dimensional studies in vitro and in vivo (Braga Silva et al., 2017). These studies aim to improve neuronal survival, axonal regeneration, and target reinnervation (Faroni et al., 2015). These models are simplistic and often limited to a culture of neurons and glia in a gel matrix. They are then assessed for cell viability and axon growth, but do not focus on physiologically significant greater organization. Often the nerve models used in these studies lack a 3D structure resembling what is seen in-vivo and do not often look to assess the more complex glial interactions such as Schwann cell myelination.

Microelectrode Array and Axonal Recordings

Microelectrode arrays (MEAs) are commonly used to study neurophysiological phenomenon at the cellular and network level. Cells are grown on top of the two-dimensional surface and come in contact with the electrodes, which are then able to record activity as well as stimulate from electrically excitable cells. The MEA we have used for these experiments has

electrodes aligned in rows of 8 by 8, totaling 64 electrodes, which were 30µm in diameter and separated by a distance of 200µm.

The commonly used neuronal culture platforms that study electrophysiology on MEAs record action potentials from the relatively large (14-75µm in diameter) DRG soma (Moreas et al., 2014) and often lack the ability for axonal interrogation, due to the smaller sizes (about 1µm in diameter) of these structures (Dworak and Wheeler, 2009; van Pelt et al., 2004). While recording action potentials from multipolar neurons such as motor neurons can be useful, there is evidence to suggest that the somas of pseudo-unipolar neurons from the DRG may not be the best location to record from. In vivo, action potentials are generated at the receptive fields for sensory neurons and they travel down afferent nerves to synapse in the CNS. While many of these action potentials do have the potential for recording and modulation at the soma, not all action potentials will (Lushcher et al., 1994). Therefore, a more accurate representation of the electrical activity from sensory nerves may be acquired from the neuronal axons.

Campenot chambers, which contain two cell culture chambers separated by thin PDMS microtunnels, have been used to separate the neuronal somas from the axons and can be used to study both structures separately (Campenot, 1994; Xiao, 2009). The tunnels are too small in width for neuronal somas to enter into and only axons and glia can traverse the distance to the second chamber. Action potentials have been recorded from two-dimensional culture systems using these devices (Dworak and Wheeler, 2009).

The aim of this study is to develop a functional three-dimensional in-vitro model of the peripheral nerve containing Schwann cell myelinated axons and appropriate microarchitecture. We have developed a functional 3-D model of the peripheral nerve using a

capillary alginate gel (Capgel™), as a scaffold. We hypothesize that: 1) The unique microcapillary structure of Capgel™ allows for the modeling of the 3-D microstructure of the peripheral nerve, and 2) That axon bundling in the capillary allows for the detection of axonal electrical activity. This system will be used to assess nerve function using an MEA to record spontaneous electrical activity. We have created 3D nerve fascicles containing myelin segments and perineurium in laminin coated Capgel™. Alginate gel is a useful material currently being used for bioengineering applications (Rocca et al., 2012; Pawar et al., 2011; Prang et al., 2006). We used a capillary alginate gel (Capgel™) as in Willenberg et al. 2011. This gel contains an excellent microarchitecture for studying the PNS with capillaries running throughout the entirety of the gel and is resorbed in-vivo. These capillary diameters can be manipulated and lumen walls derivatized with extracellular matrix proteins.

CHAPTER TWO: THE USE OF A CAPILLARY ALGINATE GEL (CAPGEL) TO STUDY THE 3D DEVELOPMENT OF SENSORY NERVES IN VITRO REVEALS THE FORMATION OF A RUDIMENTARY PERINEURIUM

Preface

This chapter was previously published in the Journal of Neuroscience Methods and is reprinted here at the permission of Elsevier.

Anderson, W. A., Willenberg, A. R., Bosak, A. J., Willenberg, B. J., & Lambert, S. (2018). Use of a capillary alginate gel (Capgel™) to study the three-dimensional development of sensory nerves reveals the formation of a rudimentary perineurium. *J Neurosci Methods*. doi:10.1016/j.jneumeth.2018.05.003

Introduction

The peripheral nerve is a three-dimensional structure with multiple levels of organization, which carry both sensory and motor information. This structure is partly established by non-neuronal cell types such as the Schwann cell (SC) and fibroblast (reviewed in Ortiz-Hidalgo and Weller, 1997 (Cravioto, 1965) (Akert et al., 1976)). SCs myelinate large caliber axons in the peripheral nerve on a 1:1 basis as well as organize unmyelinated axons into Remak bundles through limited ensheathnment. Groups of myelinated and unmyelinated axons, are embedded in

thin layers of connective tissue (the endoneurium) that is produced by endoneurial fibroblasts. Axonal groups are then organized into fascicles, bounded by several layers of flat cells forming a structure known as the perineurium. The perineurium is enriched in tight junctions and is thought to perform a function similar to that of the blood-brain barrier in the central nervous system (CNS) (Shantha and Bourne, 1968). Finally, a protective sheath called the epineurium encapsulates multiple fascicles and their accompanying blood supply.

During development of the peripheral nervous system, growing bundles of axons and their growth cones are ensheathed by SC precursors (SCPs) as they navigate to their peripheral targets (Wanner et al., 2006). At later stages of development, SCPs will undergo differentiation down the SC lineage and penetrate axonal bundles, segregating and myelinating the larger caliber axons while organizing Remak bundles for non-myelinated fibers (reviewed in (Jessen and Mirsky, 2005; Jessen et al., 2015). In contrast to myelination, the cellular origins of the sensory perineurium are not well understood (reviewed in (Kucenas, 2015). Motor axons that exit the CNS are ensheathed by CNS derived perineurial glial cells that give rise to the perineurium (Clark et al., 2014). However, these cells appear specific to motor axons and the origin of cells that make up the sensory perineurium remains unknown (Kucenas, 2015).

Cell culture models utilizing embryonic dorsal root ganglia (DRG) have been extensively used to study the growth of PNS axons and their myelination (Trotter, 1993; Wood et al., 1990). Variations of these culture systems utilize embryonic organotypic cultures as a source of early developing Schwann cells and axons (Gatto et al., 2003), or purified dissociated embryonic DRG neurons co-cultured with purified populations of Schwann cells commonly derived from the sciatic nerve (Windebank et al., 1985). Typically, these culture systems are two-dimensional and

hence do not reflect the level of architecture and organization observed in the peripheral nerve. While two-dimensional cell culture models greatly help cut the cost for drug studies when compared to live animal models, their lack of proper tissue properties such as cell-cell and cell-extracellular matrix (ECM) signaling, act as huge limitations (reviewed in (Breslin and O'Driscoll, 2013).

Neurons have also been extensively grown in three-dimensional environments in attempts to model conditions found in the brain (Breslin and O'Driscoll, 2013). With sensory neurons, requirements for the development of nerve conduits that can be used to repair breaks or damage in peripheral nerves have also resulted in numerous studies of three-dimensional axon growth in vitro and in vivo using multiple biomaterials (Braga Silva et al., 2017). These models are simplistic and often limited to a culture of neurons and glia in a gel matrix. These models are then assessed for cell viability and axon growth (Daud et al., 2012), but do not generally focus on physiologically significant greater organizational levels such as the bundling of axons into fascicles with perineurium and/or epineurium development. Such models also commonly lack complex characterization of developmental processes such as myelination.

In this study, we have cultured embryonic DRG neurons within a capillary alginate gel (Capgel™) (Willenberg et al., 2006; Willenberg et al., 2011), to exploit the capillary microarchitecture as a template for peripheral nerve growth and development. This biomaterial provides many advantages for this purpose, in that the capillary diameters can be manipulated, and the lumen walls can be derivatized with extracellular matrix proteins. Previous short-term studies (Pawar et al., 2011) have demonstrated that both axons and Schwann cells from embryonic DRG neurons are viable in this biomaterial and will migrate into the capillaries, but

did not examine further interactions between these cell types or their ability to reproduce the in vivo organization of a peripheral nerve. In our study, we have successfully derivatized the microcapillary lumen walls to encourage the growth of axons and Schwann cells and in long-term cultures have observed the production of myelinated segments. Surprisingly we also observed the formation of a rudimentary perineurium expressing tight junction components. We believe that the use of this biomaterial for sensory nerve outgrowth will provide useful insights in the study of the developing peripheral nerve.

Methodology

Animals and Reagents

All animal protocols were reviewed and approved by the Institutional Animal Care and Use Committee of the University of Central Florida. Timed (e15) pregnant Sprague-Dawley rats were purchased from Charles River Laboratories (Wilmington, MA) and euthanized by $C0_2$ inhalation according to approved guidelines. Embryos were removed and placed in a dish of Hibernate E solution. The heads were removed and the body was cut longitudinally to give access to the spinal cord with the aid of a dissection microscope.

All cell culture medium and supplements were purchased from Gibco (Waltham, MA, USA) or Sigma (St. Louis, MO, USA) unless otherwise stated in the text. The medium used for DRG culture was composed of Neurobasal, 2% B27, 1% Glutamax, 1% Pen/Strep, and freshly

supplemented with 50 ng/ml NGF (Harlan Laboratories, Indianapolis, IN). For myelination culture, 50 ug/ml ascorbic acid was added to the culture media.

Capgel™ Preparation and Derivatization

Capillary alginate gels (Capgel™) blocks were produced following the protocol of (Willenberg et al., 2006) and sliced into approximately 3x3mm blocks of 2.5mm length. Prepared Capgel™ blocks were submerged in 0.01% poly-ornithine (Sigma) solution for 4 hours at room temperature. This solution was removed and sterile gauze used to remove excess solution after which, it was submerged in a solution of 50 µg/ml natural mouse protein laminin (Invitrogen, Carlsbad, CA) in L-15 bicarbonate for 24 hours on ice. Capgel™ blocks were then moved into an incubator at 37 ºC/ 5% CO_2 overnight and the laminin solution removed and replaced with fresh culture medium. Underivatized Capgel™ was similarly prepared except dH_20 was used in place of poly-ornithine solution and laminin was not added to the L-15 bicarbonate solution.

Dorsal Root Ganglion Explant Extraction and In-Vitro Culture

Spinal cords with DRGs attached were removed from embryonic rat embryos and DRGs were then plucked from the spinal cord and pooled together in Hibernate E. Two DRGs were inserted into each Capgel™, being careful to separate them, with forceps in fresh culture medium. DRGs were inserted favoring one side to extend the distance available for nerve fascicle growth. Capgel™ blocks with DRGs were cultured in 24 well plates and given half

changes of media every 3-4 days. At 14 DIV, ascorbic acid was added to the culture medium to promote Schwann cell myelination and the culture was grown for an additional 21 days.

Tissue Processing

Cultured DRGs in Capgel™ blocks were fixed with 4% Paraformaldehyde (Electron Microscopy Sciences, Hatfield, PA) for 24 hours followed by a 30% sucrose in PBS solution for another 24 hours. Next the gels were placed in 20% OCT medium/ 30% sucrose for 24 hours, then moved to 50% OCT medium/ 30% sucrose for another 24 hours. Blocks were frozen and 10 µm serial sections were generated down the length of the block.

Tissue slices were then permeabilized in 0.2% Triton-X-100 (Amresco, Solon, OH) containing 4% PFA in PBS for 10 minutes on ice. Cells were then blocked with 10% NGS in PBS for 60 minutes at room temperature (RT) and then incubated with the following primary antibodies overnight at 4°C. Rabbit anti-Laminin antibody (1:100; Abcam, Cambridge, MA) stained laminin, mouse anti-MBP antibody (1:200; Abcam) was used as a marker to identify myelinating Schwann cells, mouse anti-β3 tubulin antibody (1:300) for neurons, mouse anti-phosphorylated neurofilament antibody (1:1500; Abcam), rabbit anti-collagen IV antibody (1:250; Abcam), mouse anti-claudin-1 antibody (1:100; Invitrogen), rabbit anti-glut-1 antibody (1:300; Abcam).

After rinsing in PBS, tissue slices were incubated for 60 minutes at RT with the appropriate secondary antibody at the following dilution: goat anti-mouse (1:2000; Life Technologies), goat anti-rabbit (1:2000). The slices were rinsed with PBS and mounted with Fluorogel (Electron Microscopy Science).

Image Acquisition and Analysis

Fluorescent images were obtained using a Zeiss LSM 710 (Carl Zeiss Ltd) confocal microscope with 488 nm and 568 nm excitation lasers. In all experiments, primary antibody omission controls were used to confirm the specificity of immunofluorescence labeling.

Statistical Analysis

Graphs included represent error with standard deviation. Statistical analysis was performed with Graphpad. Axons, myelin segments, DAPI, and percentage of myelinated axons were quantified and compared.

Findings

Laminin Derivatization Affects Nerve Fascicle Growth

The microarchitecture of Capgel™ can be appreciated in the cross-sectional image shown in Figure 4A. The DIC image illustrates that the microcapillaries of the gel, with diameters of roughly 30-50 µm, are all running parallel to each other and not intersecting one another. Laminin is a protein that helps make up the extracellular matrix and is known to promote neuronal axon growth and because of this we tested the effect of derivatizing Capgel™ with laminin on fascicle growth. Gel treated with laminin can be seen in Figure 4B where laminin has been deposited on the inner lumen surface of the gel capillaries.

Dorsal root ganglion explants were carefully inserted into Capgel™ with forceps and cultured for 35 days and then analyzed with immunohistochemistry. Figure 4C-E shows a cross section of a Capgel™ culture that was not derivatized with laminin before the culturing of DRGs at a distance of 1 mm from the explant site. DAPI shows the presence of cells in the channel, but when staining for phosphorylated neurofilament to look for neuronal axons, there was none seen. In contrast, a Capgel™ culture that was derivatized with laminin before adding DRG explants has axons present up to 1 mm from the explant, accompanied by associated glia (Figure 4F-H) present. Based on these results, all further experiments use laminin derivatized Capgel™ before DRG explants are added to the gel.

Development of an In Vitro 3D Nerve Model

DRG growth can be tracked throughout Capgel™ and by using immunohistochemistry, it can be analyzed at varying distances from the explant site through the gel. The schematic shown in Figure 5A depicts the distances from the site of DRG implantation analyzed by immune fluorescent labeling. We could identify the implant site, where many neuronal cell bodies can be found surrounded by cells that appear to resemble satellite glia, based on their location around the neuronal soma (Figure 5B). We can see here that many capillaries are being penetrated by bundles of axons around the implant site. By using Capgel™, we have the unique opportunity of tracking individual channels throughout the length of gel, in which five channels with axon bundles were chosen and analyzed at the explant site (Figure 5B) and 100 μm (Figure 5C), 500 μm (Figure 5D), and 1000 μm (Figure 5E) from the explant site.

By looking at individual nerve channels, we can appreciate that not only are axons growing through the capillaries, but they are being bundled together to give a 3D architecture. Of the channels followed through Capgel™, one channel was chosen (marked with asterisks in Figure 5B-H) and analyzed more closely. When looking at the channel 100 µm from the explant site, neuronal cell bodies are observed along with a bundle of axons and associated glia (Figure 5F). Moving further through the gel, neuronal cell bodies were not observed at distances of 500 µm (Figure 5G) or greater from the explant. Interestingly, we noticed flat cells that were localized around the outside of the axonal bundle (marked by arrows in Figure 5G) throughout the length of the gel, which based on location, reminded us of perineurial glia, which play an integral role in the nerve fascicle in vivo.

In our culture system, we add 50 µg/ml ascorbic acid at day 14 to induce collagen IV production and subsequently, Schwann cell myelination. Myelination was observed throughout the length of the gel by staining for myelin basic protein (MBP) and can be seen in the cross sections analyzed at the varying distances from the explant (Figure 5F-H). Using volume rendering of a confocal microscopy z-stack we can see the 3D nature of the nerve fascicles containing bundles of myelinated and unmyelinated axons (Figure 6A-C). In these images, we can see myelin segments and their tubular structure ensheathing axons throughout the z-stack image. The inset in Figure 6C illustrates the myelin segment wrapping around the entire axon. Longitudinal sections were also analyzed to allow for more insight into the cellular architecture (Figure 6D, E). Myelin segments were seen throughout the distance shown. The inset in Figure 3D shows a close up of a myelin segment. Based on these cellular and structural features, we

believe our system can faithfully be called an in vitro nerve model and will be referred to as such from here on forth.

Quantification of the In Vitro 3D Nerve Model

For this experiment, four Capgel™ nerve cultures were quantified from three different experiments, giving rise to 16 nerve fascicles total containing myelin, at a distance of 0.5mm from the explant site. Following these fascicles further, we observed that 10 of these grew to a distance of 1mm or more. To assess the presence of a faithfully produced 3D nerve, we selected a single Capgel™ that was treated with ascorbic acid and five channels were selected that contained axons and non-neuronal cells in multiple sections and were followed over a distance of 400µm, starting at 500µm from the site of DRG implantation. To start, we analyzed the number of non-neuronal cells present in a section of the nerve bundle, counted by DAPI (Figure 7A) and nerve fascicle diameters (Figure 7B) in each section. Next, myelin segments (Figure 7C) and neuronal axons were quantified to obtain the percentage of myelinated axons present (Figure 7D) in each tissue section and in some channels, this was found to be as high as 20% myelinated axons, which is comparable to the rat sural nerve in-vivo (Shmalbruch, 1986). This did not vary drastically over 400µm, which suggests that the same axons are being myelinated by multiple Schwann cells throughout the distance of the gel, which was also pointed out previously.

Extracellular Matrix Characterization and Perineurium Formation

To further characterize the 3D nerve fascicles, we decided to look for the presence of extracellular matrix proteins that are normally present in-vivo. Laminin is secreted in nerve fascicles in vivo and thus was analyzed in this in-vitro model. Resident cells (shown by DAPI staining in Figure 8A) and neuronal axons (Figure 8B) are surrounded by laminin (Figure 8C), which can be appreciated when these images are merged together (Figure 8D), throughout the nerve fascicle. This resembles very closely what is structurally seen in vivo.

In our in vitro nerve model, flat cells were seen lining the perimeter of the axon bundles, just like the perineurial glia do in vivo. To determine if we had developed a perineurium-like structure around nerve fascicles growing in Capgel™, we looked to characterize it with known markers of the perineurium.

We tested the effect of ascorbic acid on perineurium formation in our culture system by adding it at day 14 in our culture system. We looked for collagen IV and tight junction marker claudin-1 after 35 days in culture. In the untreated control, staining for both collagen IV (Figure 9A) and claudin-1 (Figure 9B) could be seen localized around the perimeter of the nerve fascicle. Cultures treated with 50 µg/ml ascorbic acid also had collagen IV (Figure 9C) and claudin-1 (Figure 9D) localized around the outside of the nerve fascicle and had a higher staining intensity.

A single nerve fascicle was chosen from Figure 9C and images were taken at a higher magnification to appreciate the localization of the proteins. DAPI (Figure 9E), claudin-1 (Figure 9F), and collagen IV (Figure 9G) were all seen colocalized with each other around the periphery of the nerve fascicle when the images were merged (Figure 9H). In addition to these markers, we stained for the presence of the mature perineurial glia marker glut-1 (Figure 9I). Indeed, glut-1

was present in the cells that line the outside of the nerve fascicle, proving that in this system, mature perineurial glia do line the outside of the nerve fascicle. Glut-1 staining down the nerve fascicle was looked at to appreciate its continuation (Figure10). The collagen IV localization with the tight junctional marker claudin-1 and the mature perineurial glia marker glut-1 support the idea that a rudimentary perineurium was formed in our in vitro nerve model.

Figures

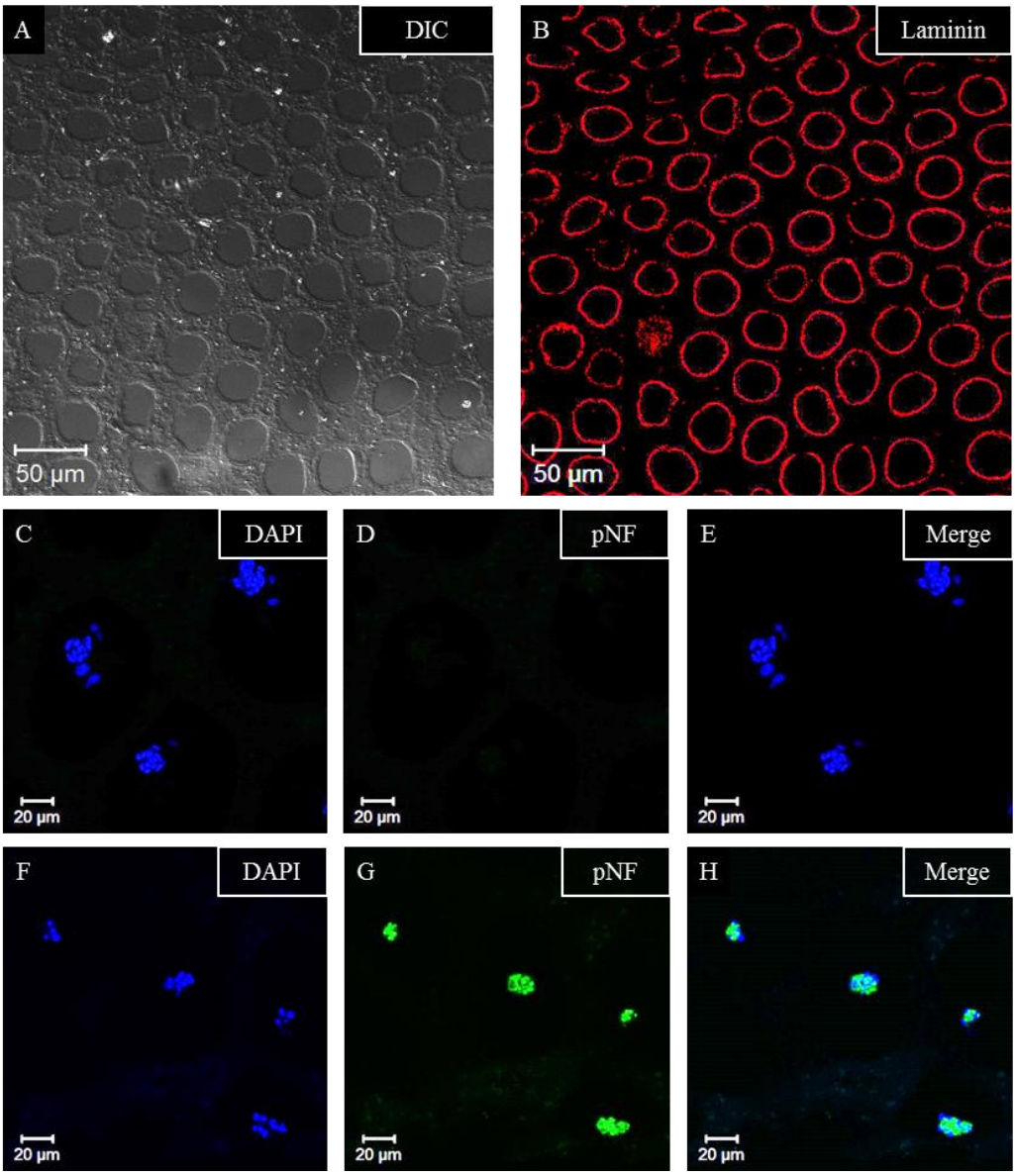

Figure 4 Laminin derivatization enhances nerve fascicle formation and growth through Capgel™.

Cross sections show the DIC (A) and laminin immunostaining (B) of a laminin derivatized Capgel™. The untreated gel (C, D, E) and laminin derivatized gel (F, G, H) are compared. Capgel™ treated with laminin have DRG neuronal fascicles 1 mm away from the explant site. Scale bars, A, B, 50µm; C-H, 20µm.

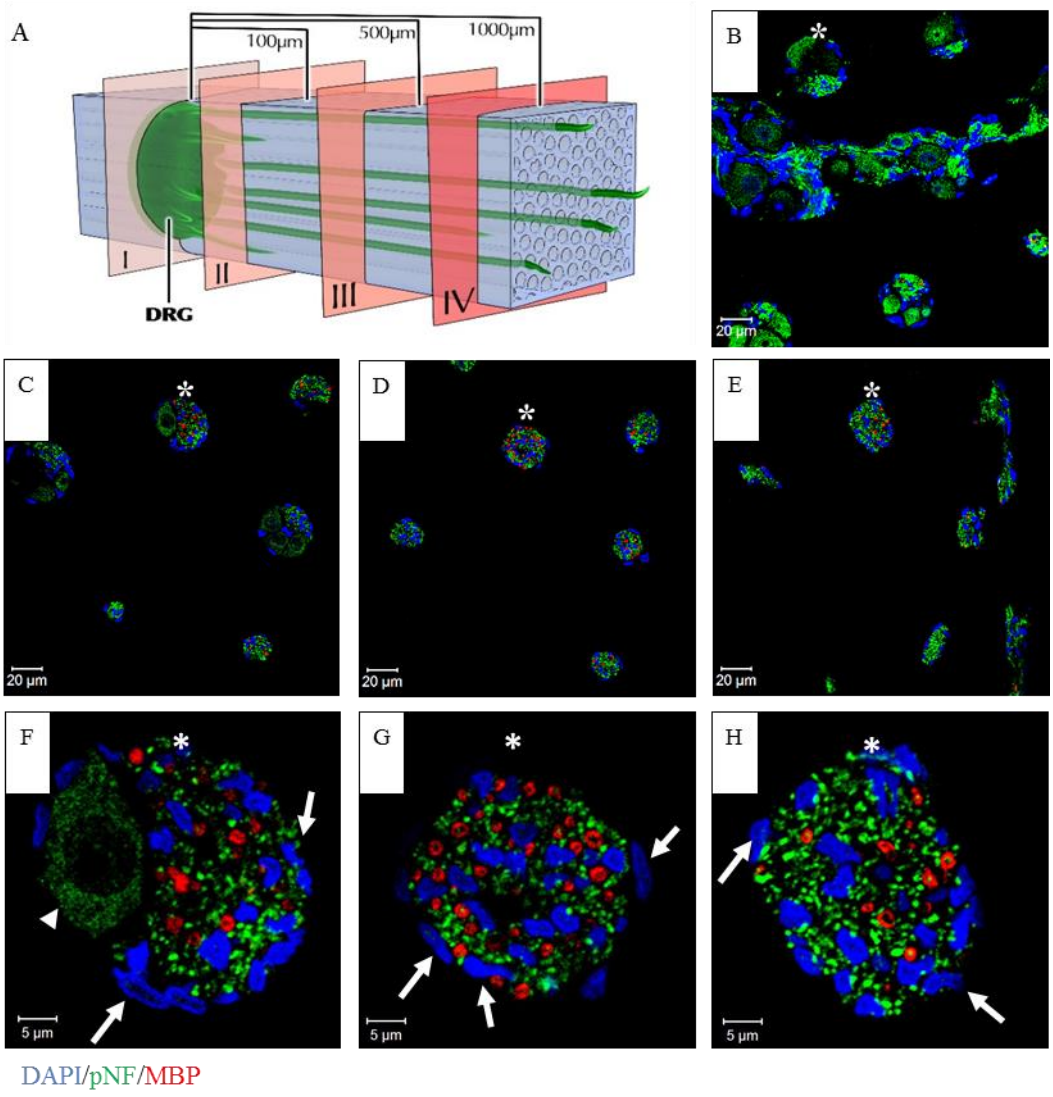

Figure 5 Analysis of Capgel™ capillaries at increasing distances from the site of explant insertion.

Illustration shows Capgel™ analysis at the DRG explant site and variable distances away (A). Five channels with myelinated nerve fascicles were selected and compared at the explant site (I, see B) and 100 µm (II, see C, F), 500 µm (III, see D, G), and 1000 µm (IV, see E, H) away from the DRG explant (IV). Asterisk marks one channel that was followed throughout the variable distance of the gel. A DRG neuron cell body is shown (arrow head) 100 µm from the explant site. We noticed flat cells around the outside of the nerve bundles, depicted by arrows. Scale bars, B-E, 20 µm; F-H, 5 µm.

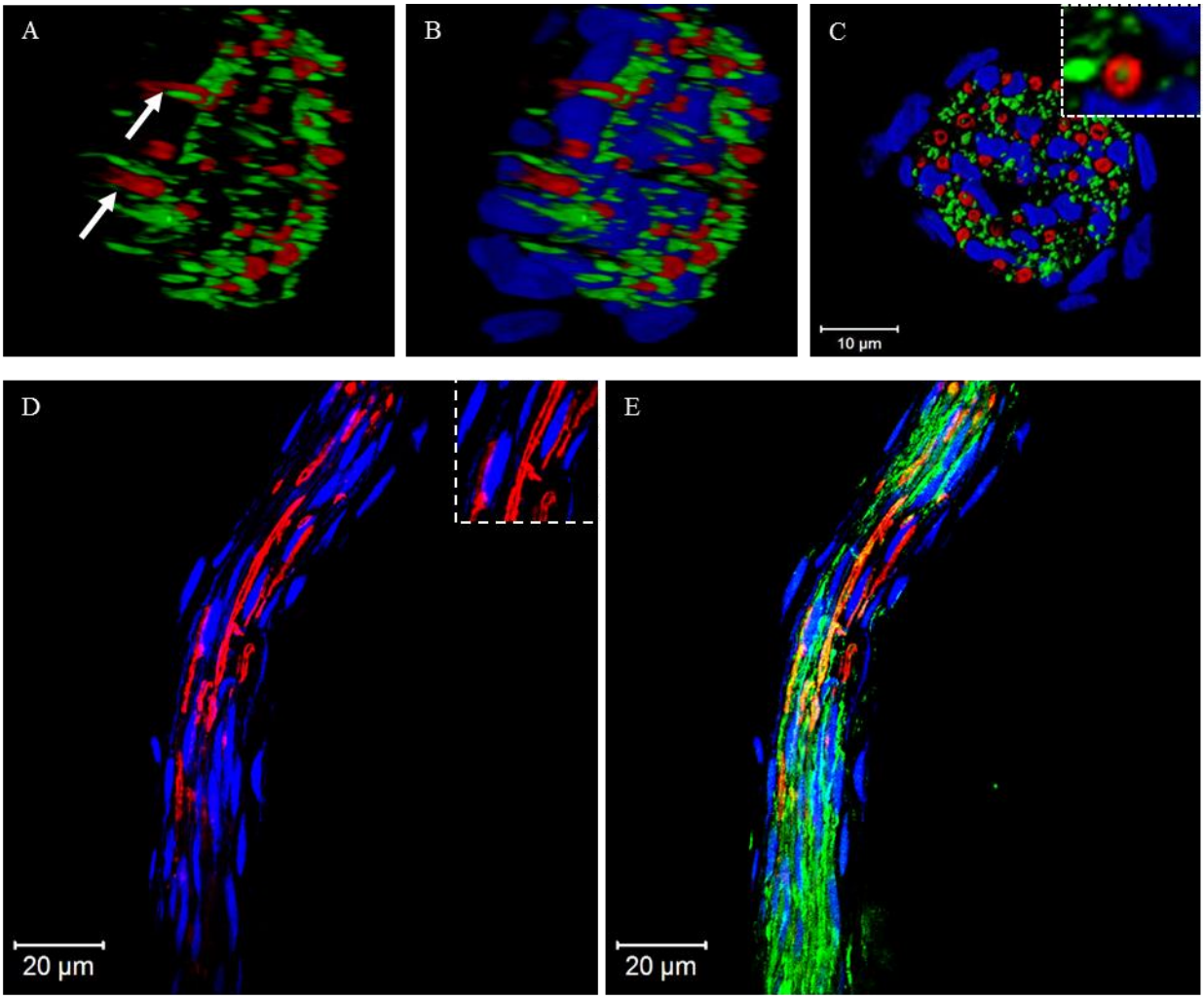

Figure 6 3D Structure of the in vitro nerve fascicle

3D rendering of a z-stack taken by confocal shows the 3D structure of a nerve fascicle (A-C). A is the same image as B without DAPI for clarity. Arrows in A point to myelin segments. Inset in C shows Schwann cell myelin around an individual axon. (D, E) Confocal image shows a longitudinal section of an in vitro nerve fascicle with myelin segments shown in red. The image in D is the same in E without pNF staining for clarity. Inset in D shows a close up of a few myelin segments. Scale bar, C, 10 µm; D, E, 20 µm..

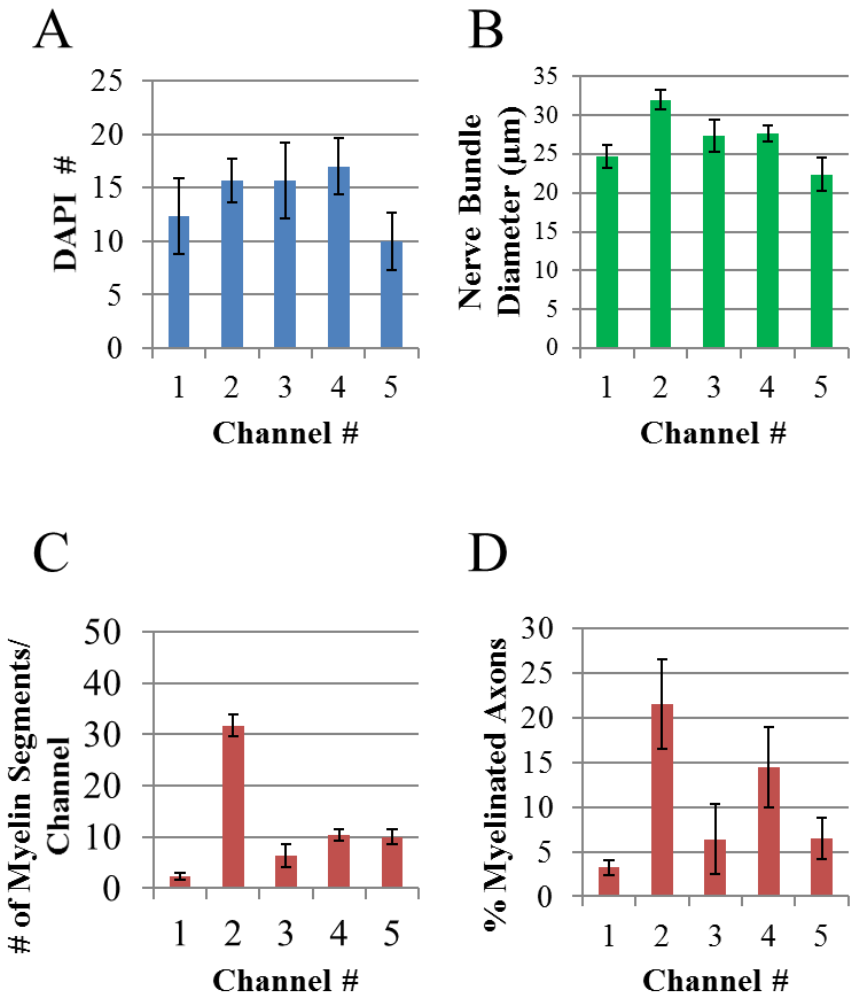

Figure 7 Nerve fascicle quantification.

Five channels with myelin segments were chosen from one ascorbic acid treated Capgel™ culture for quantification. Non-neuronal cell nuclei were analyzed and over the distance quantified (A) along with nerve fascicle diameters (B). Axons and myelin segments (C) were quantified to analyze the percent of axons myelinated by Schwann cells in each channel (D). Data was obtained from three evenly spaced serial sections over a distance 400µm at a site 500µm from the explant site. Scale bar, 20 µm.

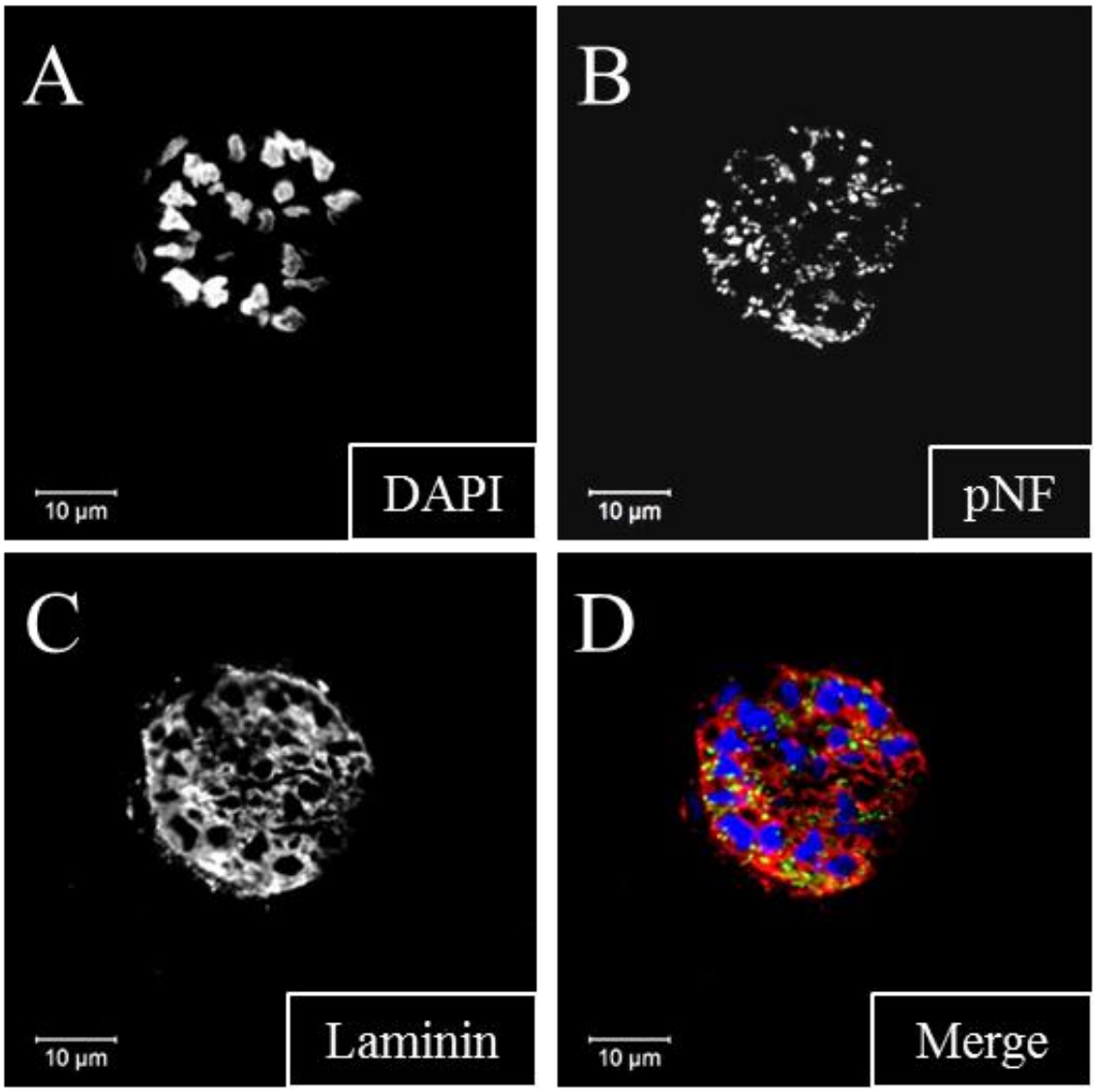

Figure 8 Laminin characterization.

Confocal images of the extracellular matrix showing laminin secreted by cells in a Capgel™ culture nerve fascicle treated with ascorbic acid. Associated glia (A) and axons (B) are found surrounded by laminin (C) throughout the nerve fascicle, which can be appreciated when these images are merged together (D). Scale bar, 10 µm.

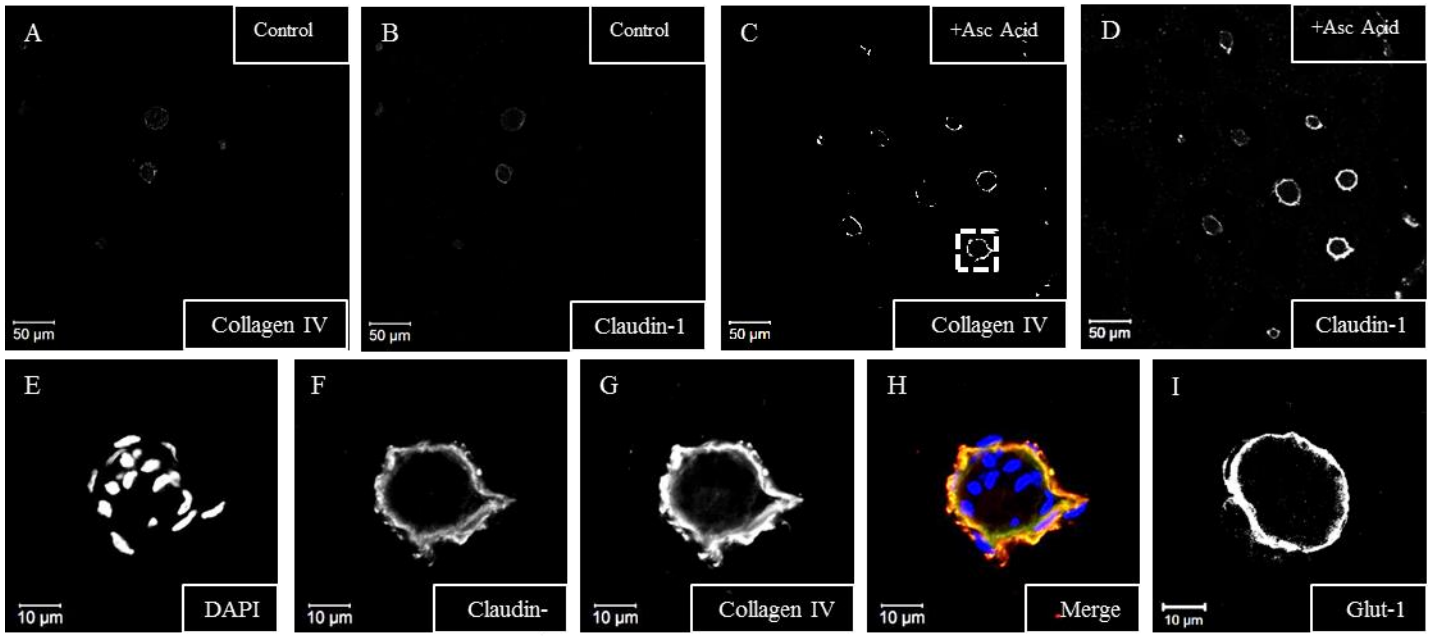

Figure 9 Perineurium formation.

Confocal images comparing Capgel™ nerve cultures untreated (A, B) or treated 50 µg/ml ascorbic acid (C, D). Collagen IV and claudin-1 staining was brighter in Capgel™s treated with ascorbic acid. One nerve fascicle was chosen in (C) and is shown at higher magnification in (E-H) to show the thick collagen IV ring colocalizing with claudin-1 tight junction staining. (I) Confocal image of the same nerve fascicle used in E-H showing Glut-1 positive+ perineurial glia are also seen around the nerve fascicle bundle. Scale bars, A-D, 50 µm; E-I, 10 µm.

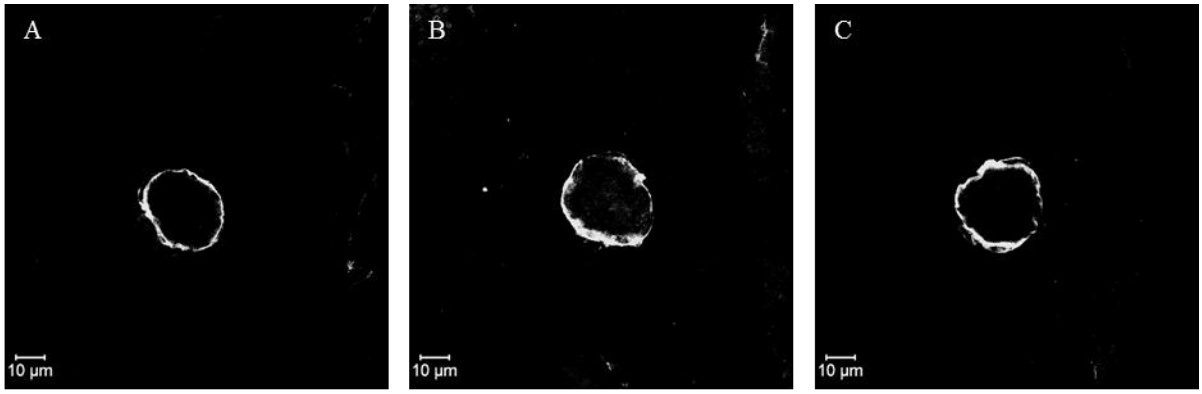

Figure 10 Glut-1 staining and continuation.

Glut-1 staining and continuation. Confocal images from a Capgel™ culture treated with ascorbic acid showing the continuation of Glut-1 staining over a distance of 100µm (A-C). Evenly spaced serial section slices were used. Scale bars, A-C, 10µm.

Discussion

We have built a 3D model of the developing peripheral nerve with the use of capillary alginate gel (Capgel™), which included structural organization similar to that seen in vivo. Axon bundles grew throughout the length of the gel, up to 1 mm from the explant and included myelinated and non-myelinated neuronal axons surrounded by a perineurium-like structure. Co-localization of collagen IV and claudin-1 with glut-1 positive perineurial glia further suggest the formation of a rudimentary perineurium. This work builds on previous work done by Pawar et al. 2011, in which a similar alginate gel was used as a substrate for DRG explant growth. These prior studies focused on the characterization of the alginate gel with a DRG culture system, but did not look at 3D nerve fascicle development or organization, Schwann cell myelination, or perineurium formation.

The microstructure of Capgel™ represents an ideal substrate for nerve fascicle growth. In contrast with the current FDA approved NGCs, which are large diameter tubes used for small gap nerve repairs, the smaller diameter channels of Capgel™ recapitulate the in-vivo nerve structure. Capgel™ is a great substrate to use and can be derivatized by extracellular matrix proteins to enhance axon bundle outgrowth, as we have done with laminin.

In vivo, peripheral nerve development starts with DRG axons bundled together with tightly associated Schwann cell precursors, which together sprout from the ganglia to reach their targets in the periphery (Reviewed by Jessen & Mirsky, 2005). Nerve fascicles grown in Capgel™ also contained bundled neuronal axons with tightly associated glia. Axons were

organized by resident glia and many of them were myelinated by Schwann cells. In vitro nerve fascicles contained the extracellular matrix proteins, laminin and collagen IV, which were localized in a manner structurally similar to what is found in-vivo. Resident glia secrete laminin in this in vitro nerve model, similar to in-vivo nerve fascicles and a thick layer of collagen IV is secreted around the perimeter of the nerve fascicle, colocalizing with flat cells that resemble perineurial glia.

In vivo, the perineurium is composed of multiple layers of flat perineurial glia that act as a nerve-blood barrier. A rudimentary perineurium formed in our peripheral nerve model We base this definition on the observation of only one to two cell layers thick around the nerve fascicle. Flat perineurial glia were found around the perimeter of axon bundles and co-localized with collagen IV and claudin-1 staining, illustrating the formation of tight junctions. In addition, glut-1 positive mature perineurial glia were found localized around the perimeter of these nerve fascicles. To our knowledge, this is the first-time in vitro nerve fascicles have been generated with a rudimentary perineurium.

Perineurium development is currently a debated topic with the key question being, from where do perineurial glia arise? Evidence for a neuroectoderm origin stems from the fact that Nkx2.2 positive cells originating from the central nervous system form the perineurium in mouse motor nerves (Clark et al., 2014). Evidence for a mesoderm lineage come from in vitro experiments that demonstrated perineurial glia are differentiated from fibroblasts, not Schwann cells (Bunge et al., 1989). In addition, in vivo experiments have shown that perineurial glia are largely not derived from the neural crest (Joseph et al., 2004). In this experiment, approximately 3% of the perineurial glia did come from the neural crest, which suggests that the perineurium

could have a heterogeneous cell population, derived from multiple sources. As of now, no one has definitively determined the origin of the perineurium in sensory nerves (Kucenas, 2015). In the presented nerve model, we have confirmed the presence of perineurial glia. Since our cultures start with only a DRG explant, it is likely that at least some cells that form the perineurium are derived from the neural crest lineage from the DRG. It would be interesting to further investigate the origin of the perineurial glia that arise from this culture in future experiments.

CHAPTER THREE: BUNDLING OF AXONS THROUGH A CAPILLARY ALGINATE GEL ENHANCES THE DETECTION OF AXONAL ACTION POTENTIALS USING MICROELECTRODE ARRAYS

Introduction

Electrophysiology is one of the preferred methods for studying nervous system function in vivo and in vitro. The patch-clamp is a method used to assess the electrical activity of individual neurons, but this technique is restricted by the number of neurons that can be studied at once, limiting its use for studying neuronal networks (Obien et al., 2015; Wood et al., 2004). The use of a microelectrode array (MEA) enables the simultaneous and long-term recording of electrical activity from a population of neurons. It is widely used to assess the electrical activity of neuronal cultures in vitro (Reviewed in Johnstone, 2010). The key advantage of the MEA is the ability to record and stimulate neurons at multiple sites, simultaneously (Obien, 2015). Through the use of this system, action potentials have been recorded and can be analyzed based on characteristics such as spike height and spike width (Narula, 2017).

Traditionally, action potentials are recorded from the neuronal somas when using an MEA. This leads to the need for culturing these neurons at high density (Newberry et al. 2016) or using patterned surfaces (Chang et al., 2000; Chang et al., 2001; Stenger et al., 1998) to ensure the neuronal cell bodies are in contact with the MEA electrode. These models lack the ability to interrogate axonal action potentials and electrical functionality, due to the small surface area (about 1 µm in diameter) of these structures (Dworak and Wheeler, 2009; van Pelt et al., 2004).

In comparison, dorsal root ganglion (DRG) neuronal somas are much larger (14-75 μm) (Moraes et al., 2014) and are more regularly studied. Studying action potentials from neuronal axons is important when working with DRG neurons, which generate action potentials at the axons and not the soma. It has been shown that action potentials generated in the axon do not always invade the soma, suggesting that the soma may not be the optimal site of action potential recording for functional studies on DRG neurons. (Luscher et al., 1994).

Campenot chambers have been used for the interrogation of neuronal axons separated from the cell bodies (Campenot, 1994 and 1977; Xiao, 2009) and action potentials have been recorded from the axons of a neuronal culture by using this chamber system in conjunction with a microelectrode array (Dworak and Wheeler, 2009). Taken together, populations of action potentials can be generated, which stem from different axons. Through waveform analysis, the spontaneous electrical activity of each axon can be studied and related back to individual recorded action potentials.

The previously mentioned in vitro models that study peripheral nerve disease are two dimensional in nature and do not sufficiently mimic the three-dimensional environment observed in vivo. Two-dimensional cell culture models lack the necessary spatial arrangements of cell and extracellular matrix organization to faithfully represent the in vivo microenvironment (Breslin and O'Driscoll, 2013). Cells in the human body naturally exist in a three dimensional architecture, which should be conserved in order to study the most accurate model of the in vivo environment and lead to the most cost effective development of drugs to fight these diseases. In Chapter 2, we described the development of a three dimensional model of the peripheral nerve in vitro, complete with myelinating Schwann cells and a rudimentary perineurium using a capillary

alginate gel (Capgel™), which better mimics the microstructure seen in vivo (Anderson et al, 2018; and Chapter 2). As complete a model as this was structurally, it lacked any functional measurements, such as electrical activity of the neuronal network. Interestingly, our nerve model generated tightly bundled axons that grow through the end of the gel block. Also of note, the neuronal cell bodies have limited migration through the gel block. This separation of neuronal soma from axon bundles provided us the perfect tool to assess the ability to record axonal action potentials and look to see if bundling of the axons will allow for the recording of action potentials above a detectable threshold.

We show here the novel use of a tissue engineered three-dimensional in vitro model of the peripheral nerve and the unique features the bundled axons provide by integrating capillary alginate gel (Capgel™) with a microelectrode array (MEA) to record spontaneous activity in axon bundles. By using this gel, we have separated the neuronal cell bodies from the axons in a manner similar to the Campenot chamber, ensuring that only axons interface with the MEA and not neuronal soma. By taking advantage of the three-dimensional structures generated using this model, action potentials were recorded from axon bundles interfacing with the MEA electrodes and were analyzed using waveform analysis. Through analysis of the action potentials recorded we were able to decipher between multiple individual action potentials from separate axons in one axon bundle contacting the MEA. Further, we showed a varied response of the neurons to the TRPV1 agonist capsaicin, often implicated in pain stimulus signaling, which we measured based on action potential profiles.

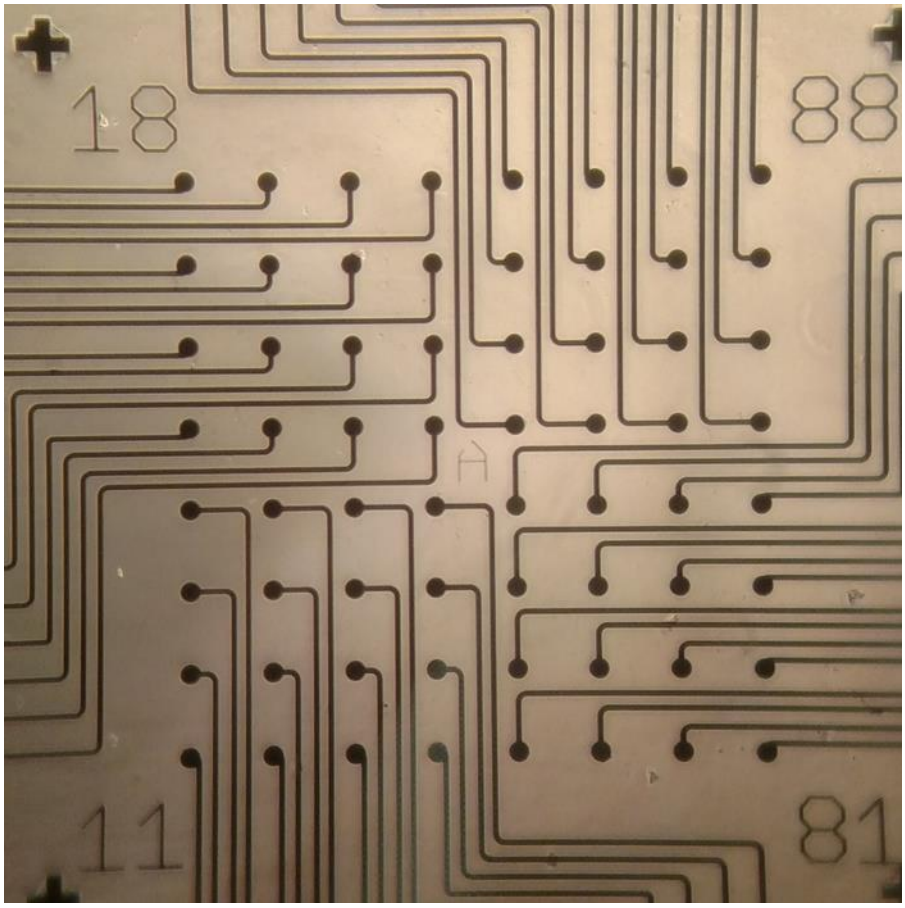

Figure 11 Axion microelectrode array

Image shows the surface of a pretreated MEA before the addition of cells. The 64 electrodes are 30 µm in diameter and separated by 200 µm, center to center.

Methodology

Animals and Reagents

All animal protocols were reviewed and approved by the Institutional Animal Care and Use Committee of the University of Central Florida. Timed (e15) pregnant Sprague-Dawley rats were purchased from Charles River Laboratories (Wilmington, MA) and euthanized by CO_2 inhalation

according to approved guidelines. Embryos were removed and placed in a dish of Hibernate E solution. The heads were removed and the bodies cut longitudinally to give access to the spinal cord with the aid of a dissection microscope. Thoracic DRGs were removed and used for all experiments.

All cell culture medium and supplements were purchased from Gibco (Waltham, MA, USA) or Sigma (St. Louis, MO, USA) unless otherwise stated in the text. The medium used for DRG culture was composed of Neurobasal, 2% B27, 1% Glutamax, 1% Pen/Strep, and freshly supplemented with 50 ng/ml NGF (Harlan Laboratories, Indianapolis, IN).

Capgel™ and MEA Preparation

Capillary alginate gel (Capgel™) was received from Dr. Bradley Willenberg and created following the protocol from Willenberg et al., 2011 and derivatized with laminin following the protocol from Anderson et al., 2018. Capgel™ is submerged in 0.01% poly-ornithine solution for 2h at room temperature on a shaker. This is followed with an incubation for 2h at 4^0C on a shaker. This solution is removed and sterile gauze is used to remove excess solution still in the gel, while on ice. After which, the gel is submerged in a solution of 50µg/ml natural mouse protein laminin (Invitrogen, Carlsbad, CA) in L-15 bicarbonate on ice then moved to a shaker at 4^0C for approximately 48 hours. Capgel™ is then moved into an incubator at 37ºC/ 5% CO_2 for 5h.

64 electrode single well MEAs (Figure 11; M64-GLx, Axion BioSystems, Atlanta, GA) were treated with 0.01% poly-L-ornithine (Sigma, St. Louis, MO) solution for 1h at RT. The solution is then removed and the MEA is placed on an inverted 100 mm plate lid on ice. The MEA

surface is then treated with 50µg/ml laminin solution and moved to the incubator at 37°C/ 5% CO_2 overnight. Excess unbound laminin solution is removed from the MEA surface and quickly replaced with fresh culture medium at RT. Capgel™ is placed directly on top of the electrodes of the MEA with channels aligned vertically.

Cell Culture

Four DRGs were carefully added to the top of a Capgel™ block sitting on the MEA and allowed to adhere to the Capgel™ surface. Care was taken to ensure the Capgel™ block covered the entire 64 electrodes of the MEA and that the channels were oriented perpendicular to the surface. The capillary channels were at a density of approximately 40 channels/ mm^2 and no effort was made to ensure that capillary channels lined up with MEA electrodes. DRGs extend axon bundles through the gel capillaries and make contact with the MEA at around 11-15 DIV. Starting at day 5, the electrical activity was recorded on the MEA for 10 minutes every two days. Half the culture medium is replaced every two days, after the MEA recording is taken.

Capsaicin Treatment of Dorsal Root Ganglia Cultures

1µM Capsaicin (Sigma) in DMSO (Sigma-Aldrich, St. Louis, MO) was directly added to the culture medium at 21 DIV and recorded for 5 minutes. Comparable controls were established by adding equivalent volumes of DMSO without Capsaicin.

Culture Tissue Analysis

Capgel™ cultures were fixed with 4% Paraformaldehyde (Electron Microscopy Sciences, Hatfield, PA) for 18h followed by a 30% sucrose in PBS solution for another 24h. Next, the gels were placed in a solution of 20% OCT medium/ 30% sucrose for 24h, then moved to 50% OCT medium/ 30% sucrose for another 24h. Gels were frozen in OCT and serial sectioned at 10µm thick sections on a cryostat.

Tissue slices were then permeabilized in 0.3% Triton-X-100 (Amresco, Solon, OH) containing 4% PFA in PBS for 10min on ice. Cells were then blocked with 10% NGS in PBS for 60min at room temperature (RT) and then incubated with the following primary antibodies overnight at 4°C: Rabbit anti-Laminin antibody (1:100; Abcam, Cambridge, MA) stained laminin and mouse anti-β3 tubulin antibody (1:300) for neurons.

After rinsing in PBS, tissue slices were incubated for 60min at RT with the appropriate secondary antibody at the following dilution: goat anti-mouse (1:2000; Life Technologies), goat anti-rabbit (1:2000) and DAPI (1:200). The slices were rinsed with PBS and mounted with Fluorogel (Electron Microscopy Science).

Image Acquisition and Analysis

Fluorescent images were obtained using a Zeiss LSM 710 (Carl Zeiss Ltd) confocal microscope with 488nm and 568nm excitation lasers. In all experiments, primary antibody omission controls were used to confirm the specificity of immunofluorescence labeling.

Statistical Data and Analysis

Electrical readings were recorded using the 2.1.1.16 Axion Integrated Studio (AxIS) software for 10 min every two days with the heating element set to 37°C. Adaptive threshold crossing at six standard deviations with a pre-spike of 0.84ms and post-spike of 2.16ms was used. Data from all 64 electrodes was recorded. Axion spike files were analyzed using the 2.0.4 Neural Metric Tool (Axion Biosystems). Electrodes with a firing rate of ≥ 5spikes/min were included in the analysis. Mean firing rate was calculated as the average firing rate across 64 electrodes and weighted firing rate was calculated as the average firing rate of the active electrodes. A custom MATLAB script was used for further analysis of extracted waveforms: a standard principle component analysis was applied to 11 characteristics of recorded waveforms (including e.g. peak-to-peak height, spike width at half-max as well as positive and negative slopes) in order to sort different shapes of action potentials with the kmeans algorithm Figure 17A). Subsequent analysis was performed under the premise that individual clusters of waveforms originated from different neurons/neurites and were hence treated as individual data set (Egert, Knott et al. 2002, Wiltschko, Gage et al. 2008)Wiltschko et al., 2008; Egert et al., 2002). Every neuron's firing frequency was tracked over time via reciprocal inter-spike-intervals and plotted as a log-transformed, box-filtered histogram (Figure 17B). The peak maxima were defined as the firing rate of respective neurons. Mean firing rates were calculated as the average firing rate across all 64 electrodes on an MEA and weighted firing rates were defined as the average firing rates of only the active electrodes.

Findings

Developed Functional In-Vitro 3D Nerve Model by Integration with MEA

Dorsal root ganglion were cultured on top of Capgel™ blocks and axon bundles penetrated the capillaries and grew through to the bottom of the gel. A schematic of a typical culture is depicted in Figure 12A, showing the Capgel™ directly on top of the electrodes of the MEA. DRGs growing on top of the Capgel™ are shown extending bundles of axons through the gel capillaries and through to the other side of the gel, where the bundles come in contact with the electrodes. A tissue section is shown in Figure 12B and further magnified in Figure 12C, which is taken from the point of axon bundles penetrating the capillaries. DRG neuron cell bodies can be seen here, which have migrated into the capillaries with the axons and glia. Cells surrounding the DRG cell bodies whose location suggests that they may be satellite glia were also observed. The maximum distance at which neuronal cell bodies were found was approximately 400µm from the top of the gel (data not shown). Tissue sections taken at the end of the gel, nearest the point of axon bundle integration with the MEA electrodes, show the axon bundles right before they reach the end of the gel, which is about 2mm from the DRG explants (Figure 12D, E). Importantly, there are no neuronal cell bodies at this point, which means that only axon bundles and glia come in contact with the MEA. The axon bundles grew through the entire length of the Capgel™ block and the capillary diameter was about 100µm ($\bar{x}$102.12 ± 22.10µm, n = 5, Figure 12F). As the bundles exited the capillaries, they were around 8µm ($\bar{x}$8.02 ± 0.57µm, n = 5) in diameter (single axons are typically less than 1µm in diameter) and appeared to make contact with the electrode (Figure 12F). Different waveform (WF) units on each individual electrode

were analyzed using clustering criteria as described in the materials and methods section (Figure 17). The waveforms that resulted from the action potentials of each neuron will be characteristic and so, the number of distinct waveform units on each electrode will indicate the number of individual neurons contributing to the electrical activity on that electrode. Figure 12G shows that about 92% of the electrodes analyzed (n = 588) had three or more waveforms, suggesting that multiple different axons within the same bundle are contributing to the firing observed at a single electrode.

Experimental Set Up for Comparison of 2D and 3D Culture Experiments

To compare electrical activity recorded by the MEA from different parts of the neurons, a variety of two-dimensional DRG culture experiments were compared with the three-dimensional Capgel™ culture, the setup of which is illustrated in Figure 13. To start with, we cultured DRG explants directly on top of the MEA electrodes, so that each DRG covered a different quadrant of the electrodes (Figure 13A). This culture had DRG neuron cell bodies and axons in contact with the electrodes, though it is only action potentials from the neuronal cell body that were expected to be recorded and not from the axons.

Typically, it is proposed that action potentials from neuronal axons in contact with the electrodes of a MEA in a two-dimensional culture are too small to be recorded. To test this, we devised a system where we placed the DRG explants on the outside corners of the MEA, where they would not be in contact with the electrodes (Figure 13B). After a few days in culture, axons grew out from the explants and covered the electrodes. In this set up, only axons and associated glia came in contact with the electrodes, not the neuronal cell bodies.

Figure 13C shows an image of the Capgel™ culture sitting on top of the MEA electrodes. Care was taken to ensure that the gel completely covered all of the electrodes and many of the capillaries present appeared darker through phase microscopy, suggesting that they were infiltrated by many cells and axons. The spontaneous firing rate from these three-dimensional cultures was then compared with the two-dimensional cultures.

Bundling of Axons Results in Dramatically Higher Firing Rates

Comparison of the well-wide mean firing rate between the somatic ($\bar{x}$ 0.02, n = 6), single axons ($\bar{x}$ 0.01, n = 8), and bundled axons ($\bar{x}$ 0.18, n = 6) (using Capgel™) from the first day of firing (1DF) to 11DF revealed that bundled axons have a firing rate that is significantly greater than the somatic ($p = 0.026$) and single axon readings ($p = 0.010$) (Figure 14A) indicating that a high number of the Capgel™ bundled axons generated action potentials exceeding our threshold settings. There was negligible electrical activity seen where single axons made contact with the MEA electrodes, but the bundling of axons generated consistently higher readings when compared with the two-dimensional cultures. The Capgel™ bundled axon condition started off with low well-wide mean firing rate, as fewer bundles made contact with the electrodes. This is reflected in the small number of active electrodes during early time points (data not shown). With time, there was an increase in the well-wide firing rates that peaked between 9DF and 13DF (Figure 14B).

Figure 14C shows a representative image of waveform units that were recorded on a single electrode in the three different experimental designs. We were able to identify distinct waveforms in the neuronal soma, as well as from single and bundled axons. Single axons have

waveforms that are typical of noise (these units have the same shape in both positive and negative directions and these spikes were not considered for further analysis) and less than ten data points were available for axonal measurements. Somatic spikes are known to be wider than axonal spikes (van Pelt et al., 2004; Buitenweg et al., 2002) and our analysis of the waveforms indicated a significant difference in the width of spikes between the soma ($\bar{x}$ 0.24 ± 0.01ms, n = 42) and single axons ($\bar{x}$ 0.21 ± 0.01ms, n = 8, $p = 0.020$) as well between the soma and bundled axons ($\bar{x}$ 0.19 ± 0.00ms, n = 91, $p < 0.0001$). No significant difference was observed between the single and bundled axons ($p = 0.331$), further establishing the idea that the cell bodies did not contribute to the detected signals and that only axons were present at the interface of Capgel™ block and the MEA (Figure 14D). Interestingly, we did not see an amplification of the voltage for the bundled axons (Figure 14E, $\bar{x}$ 31.99 ± 1.22µV, n = 93) that has been reported by other groups that attempted to acquire axonal readings using microtunnels (Dworak and Wheeler, 2009; Narula et al., 2017; Lewandowska et al., 2015).

In our three-dimensional system, the bundles of axons that made contact with the electrodes continued to maintain the same connections with time because the Capgel™ block is stationary throughout the experiment. This was advantageous because we could monitor the electrical activity of the same bundle of axons long-term. We show in Figure 15, the same electrode tracked for 24DIV, starting at 11 DIV. Three distinct units of waveforms that consistently appeared over this period and the firing rate of each of these units is shown. Although the firing rate of these individual units changed over this period of time, the spike shapes were overall remarkably consistent and reproducible. Slight changes in the spike shapes that were observed could be as a result of developmental or maturation differences as

previously reported (Lewandowska et al., 2015). This model can be used as a tool to study and understand these changes.

Bundles of Axons Within The Capgel™ Blocks Are Comprised of a Heterogeneous Population Of Axons Similar to an In Vivo Nerve

DRG are composed of several different types of neurons: nociceptive, mechanoreceptive, and proprioceptive, which are involved in transmitting different types of sensory inputs to the CNS (Scott, 1992; Montano et al., 2010; Marmigere and Ernfors, 2007). To further study the composition of the axon bundles formed within the Capgel™ capillaries, we added capsaicin, a TRPV1 receptor agonist, to the culture, in order to model pain (Caterina et al., 2000; Caterina et al., 1997; Heinricher et al., 1987; Tominaga et al., 1998). Figure 16A shows the weighted firing rate for the DMSO control and the firing rate after the addition of capsaicin at 21DIV. We see here that the addition of capsaicin led to an overall increase in the mean firing rate (control $\bar{x}$ 3.01 ± 0.33, n = 4; capsaicin $\bar{x}$ 10.49 ± 2.23, n = 4, p = 0.016). This increased firing rate in response to capsaicin treatment is well documented (Newberry et al., 2016; Caterina et al., 2000; Wainger et al., 2015). Analysis of the waveforms indicated a change in the firing rates with no changes in the voltage (p = 0.631, data not shown). Electrode level analysis was then performed to further investigate the response of individual electrodes to capsaicin treatment. Here, we show that about 14% of the electrodes analyzed showed no increase in their mean firing rates in response to capsaicin (Figure 16B) and further, we show that responsive electrodes had a varying degree of response to the treatment (Figure 16B, C). This suggested that the electrodes had different ratios of nociceptive neurons interfacing with them (Caterina et al., 2000). To further

investigate how individual axons within a bundle responded to capsaicin treatment, we teased out each unit of waveform on individual electrodes. Analysis of electrode 39 indicated three distinct waveforms that we refer to as unit 1 (green), 2 (blue) and 3 (yellow). We show here that the waveforms remain unchanged after capsaicin treatment (Figure 16D) and this allowed us to investigate their individual frequencies in response to capsaicin (Figure 16E). Here we see that unit 1 (control $\bar{x}$ 1.04 ± 0.26, n = 77; capsaicin $\bar{x}$ 10.37 ± 1.07, n = 633, p = 0.008) and unit 3 had a significant increase in response to capsaicin (control $\bar{x}$ 4.52 ± 1.53, n = 146; capsaicin $\bar{x}$ 12.89 ± 0.89, n = 936, p = 0.001) whereas unit 2 showed no response to capsaicin control ($\bar{x}$ 8.81 ± 6.15, n = 71; capsaicin $\bar{x}$ 9.31 ± 0.86, n = 588, p = 0.883). This suggested that unit 1 and 3 were sensitive to capsaicin indicating that they were nociceptive in nature, whereas unit 2 could be a different subclass of DRG neurons, which lack the TRPV1 receptors.

Figures

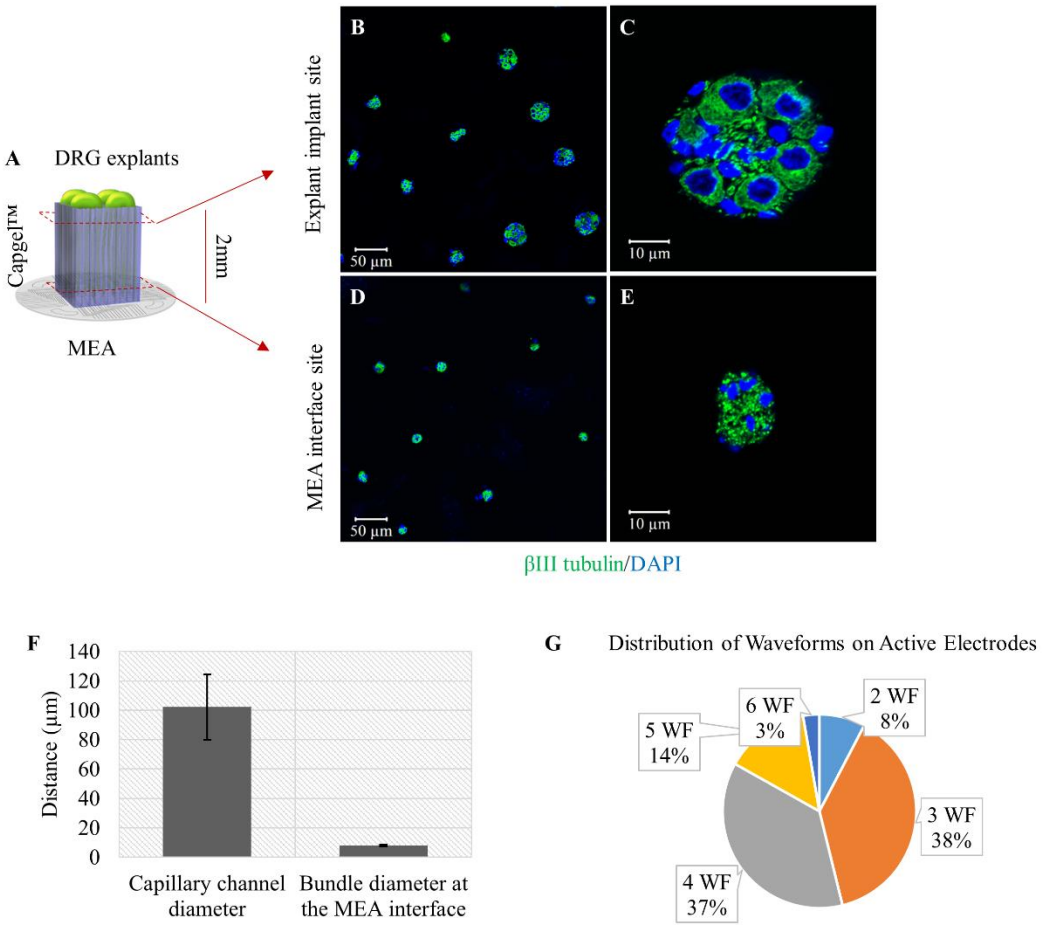

Figure 12 Integration of 3D nerve Capgel™ culture with a microelectrode array set up.

Illustration shows Capgel™ placed on a MEA with DRG nerve fascicles growing through the gel. Confocal images of cross sections of the gel show the explant entering the gel (B, C) and also at a site 2mm from the explant site where the axonal bundles, comprised of axons in green (β-3 Tubulin) and associated glia nuclei are blue (DAPI), come in contact with the MEA (D, E). Capillary diameter and axon bundle diameters coming into contact with the MEA were measured (F). Chart shows the distribution of wave forms on active electrodes (G). Scale bars, B, D, 50µm; C, 10µm; E, 5µm.

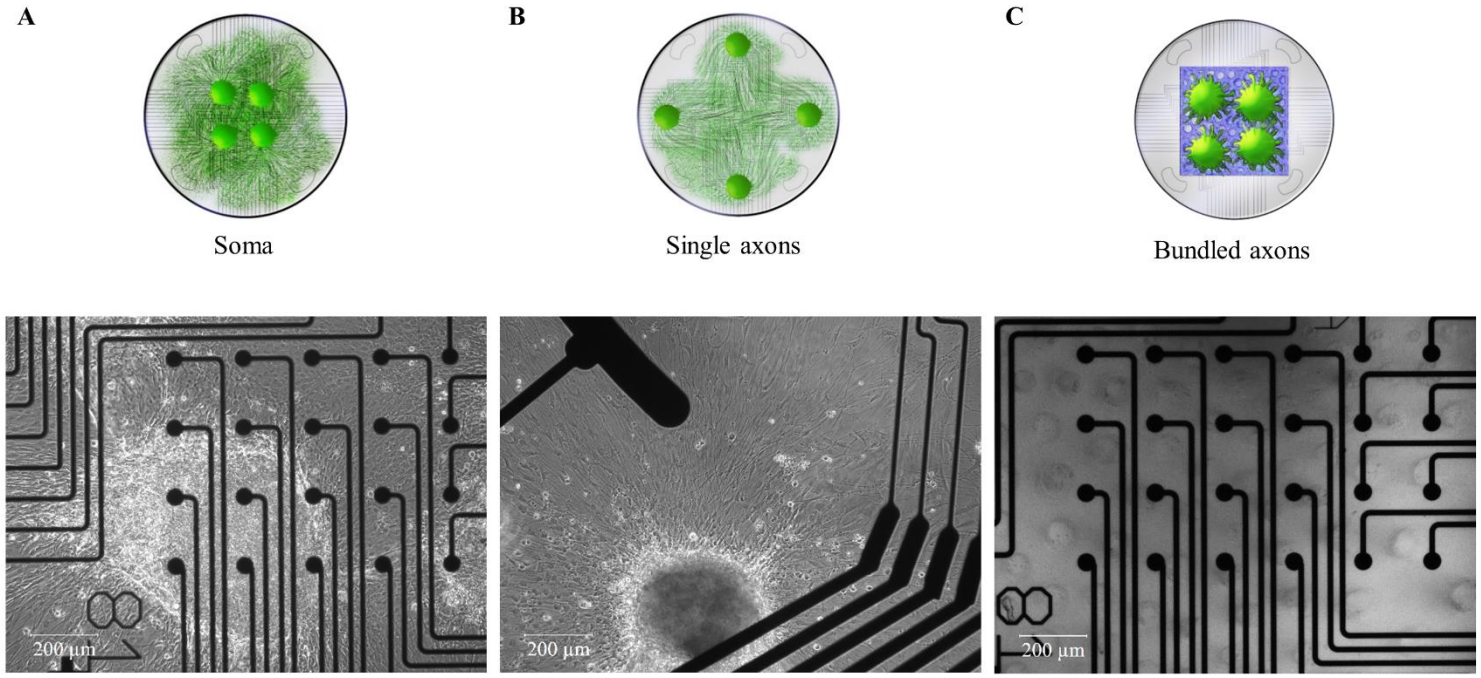

Figure 13 Experimental conditions for the comparison of neuronal somas, axons, and bundled axons on an MEA.

(A) Neuronal soma experiment is depicted showing DRG explant plated directly on the MEA surface, so that each DRG roughly covered the area of one quadrant. (B) To record from single axons, DRG explants were placed at the corners of the MEA, ensuring that neuronal somas did not come in contact with the electrodes. (C) Recorded electrical activity from bundled axons was achieved by placing the Capgel™ culture directly on top of the electrodes.

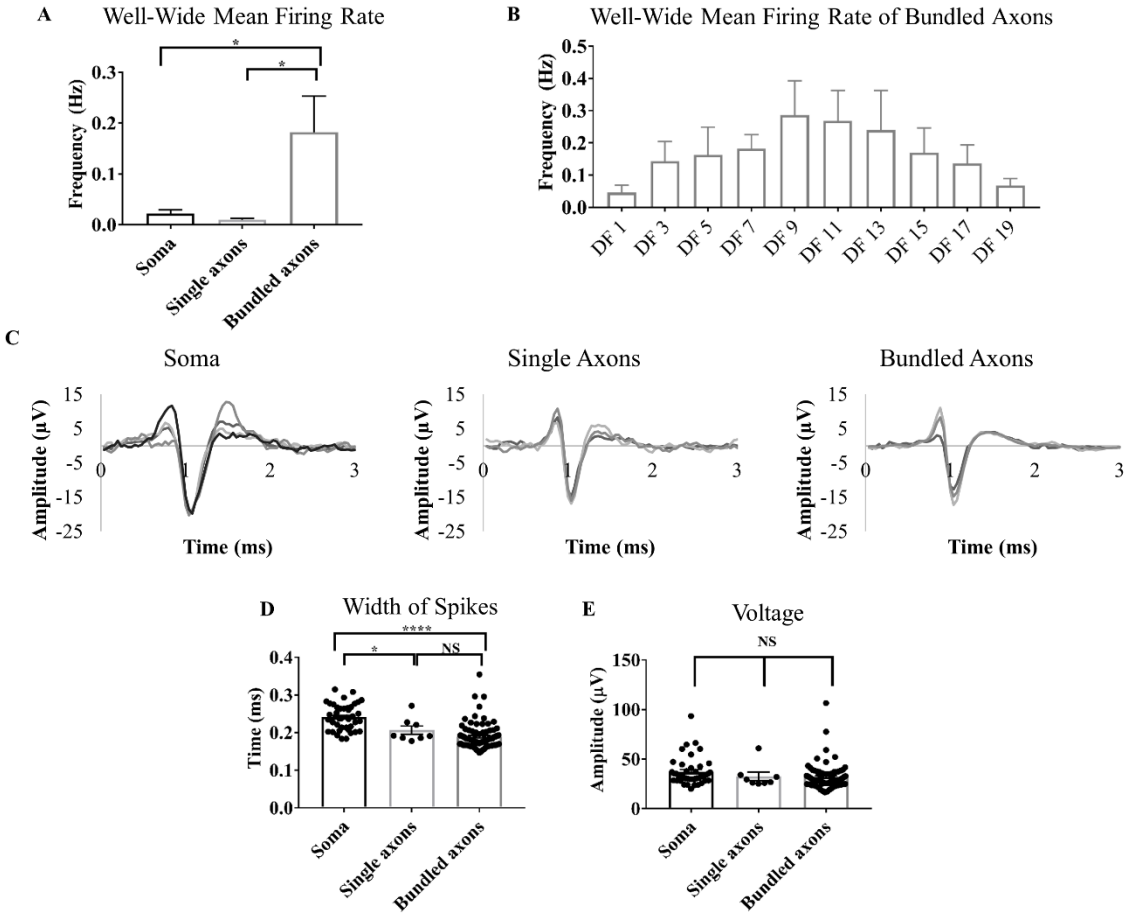

Figure 14 Bundling of axons in 3D yields firing rates dramatically higher than comparable two-dimensional cultures.

(A) Well-wide mean firing rates of the different experimental groups. The data is represented as a mean across all 64 electrodes (analyzed by one-way ANOVA with Tukey's multiple comparisons test; error bars represent SEM, *$p \leq 0.05$). (B) Analysis of well-wide mean firing rate of bundled axons from Capgel™ culture. (C) Representative wave forms for each experimental condition. Each line represents a unit of spikes that have consistently fired and clustered as a distinct waveform. (D) Comparison for the width of spikes and (E) voltages between conditions. Data analyzed by one-way ANOVA followed by Tukey's multiple comparisons test; error bars represent SEM, ****$p \leq 0.0001$, *$p \leq 0.05$.

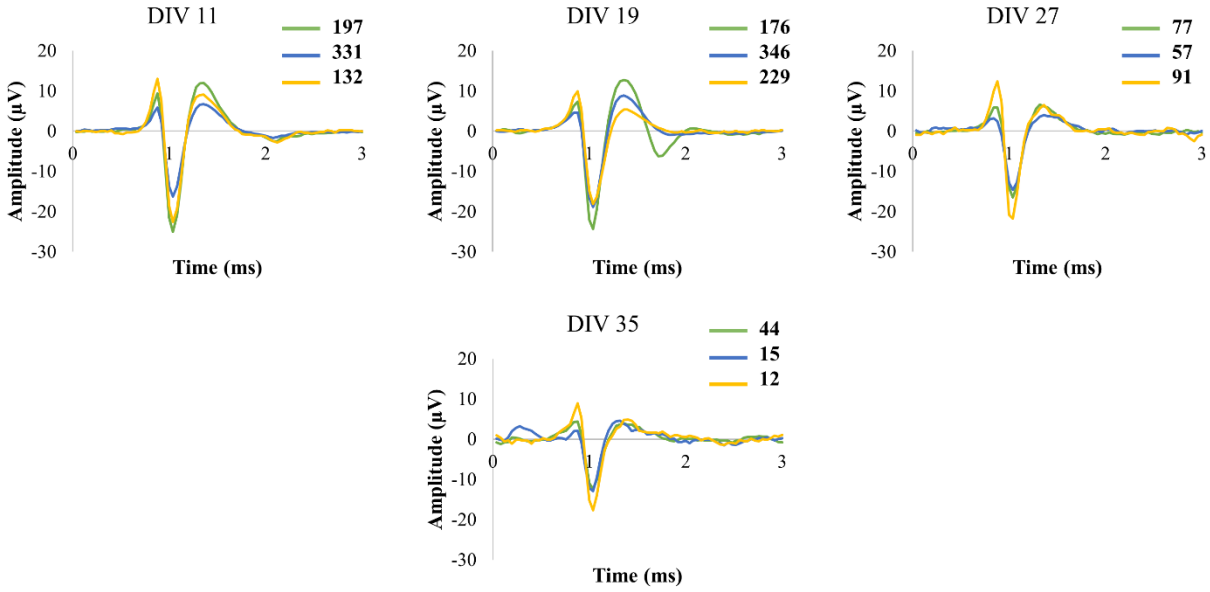

Figure 15 Long term recording of bundled axons in vitro.

Waveforms recorded on a single electrode from 11 DIV to 35 DIV. The total number of times each waveform unit fired is indicated.

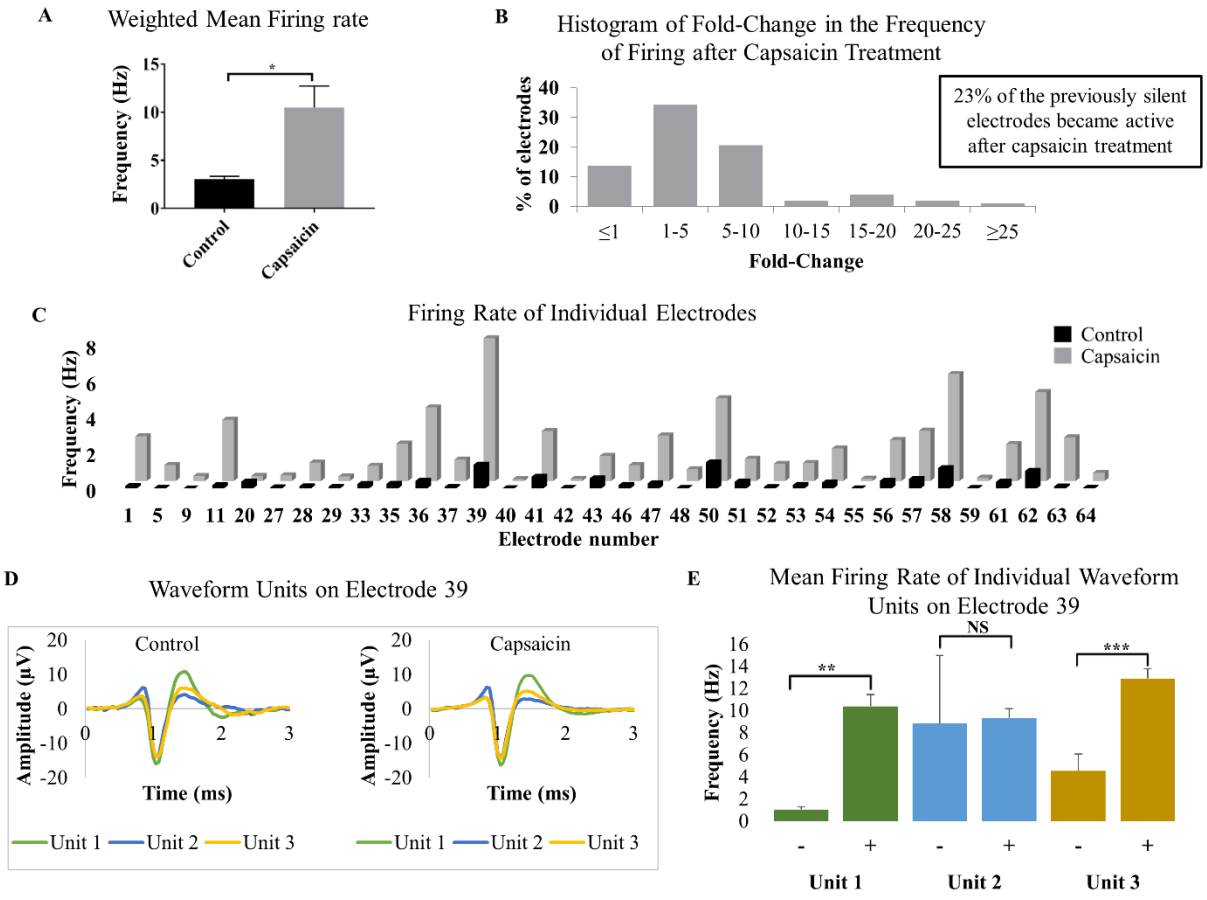

Figure 16 Analysis of electrical activity in response to capsaicin treatment.

(A) Weighted mean firing rate (data analyzed by paired t-test; error bars represent SEM, *$p \leq 0.05$. (B) Distribution of electrodes showing fold-changes in the frequency of firing. (Mean firing rate of individual electrodes in response to capsaicin treatment from a single experiment. (D) Analysis of waveform units on electrode 39. (E) Mean firing rate of individual waveform units were analyzed using the bootstrap t-test; error bars represent SEM, **$p \leq 0.01$, ***$p \leq 0.001$.

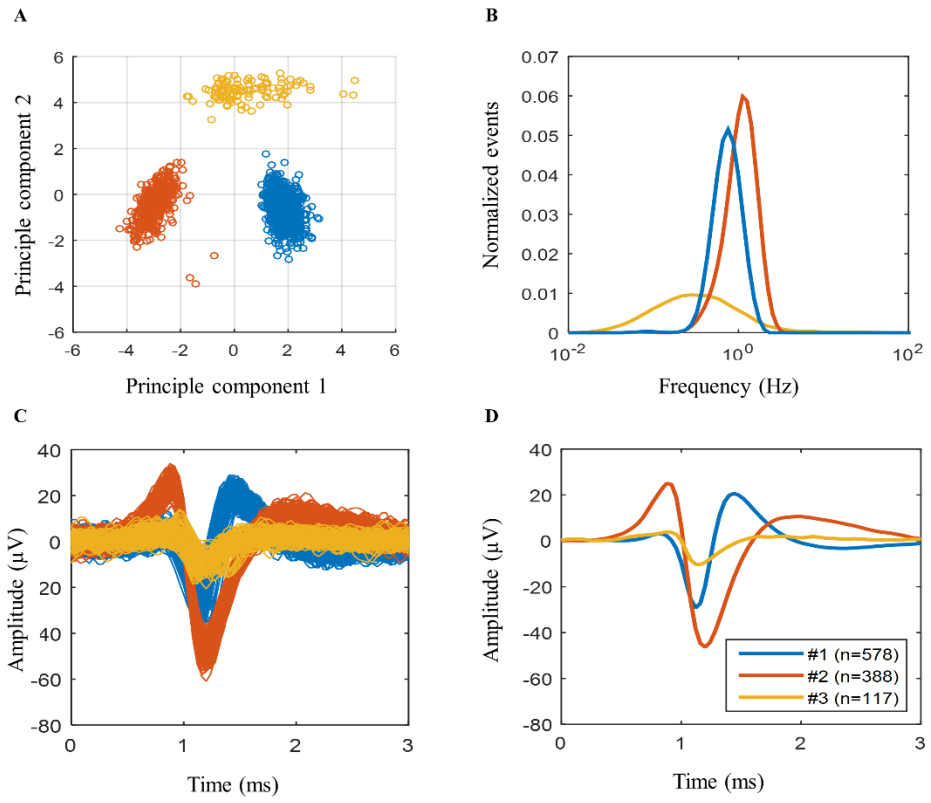

Figure 17 Waveform analysis.

(A) kMeans clustered principle components of waveforms after the reduction down to two components (down from eleven). (B) Logarithmically plotted, box-filtered frequency histograms for each cluster of action potentials. (C) Superimposition of action potentials from the clusters shown in A. (D) Mean waveforms of clustered action potentials.

Discussion

We have integrated our 3D in vitro nerve model with a microelectrode array to create a functional nerve model. The bundling of axons with Capgel™ allowed for the detection of axonal activity with the use of an MEA We have shown here that this bundling of axons through Capgel™ greatly improved our recording of spontaneous electrical activity from DRGs. We have also showed that this system allows for the long-term monitoring of electrical activity in vitro. Finally, we show here that based on the electrical data presented that the axon bundle composition is heterogeneous, with individual action potentials and their responses to capsaicin discernable, similar to what is observed in vivo.

There has been recent interest in acquiring axonal action potential readings in vitro, but these methods generally require either patterning or complex modification of the MEA surface. The model described here requires no modification to the commercially available MEA and instead we used a cheap and easily synthesizable biomaterial to generate bundles of axons, which can be placed on top of the MEA surface. Importantly, most of the established models used to record from neuronal axons lack the structural three-dimensional complexity that is observed in vivo. Using Capgel™, we have, in essence, created a three-dimensional Campenot chamber-like device, which ensured neuronal cell bodies were kept separate from the axonal bundles that grew through the end of the gel block. We were able to generate a three-dimensional structure, which offered a more realistic composition in which the functional properties of neurons can be replicated and observed.

Two dimensional microtunnel systems that are able to detect axonal action potentials work off the idea of concentrating axons into the smaller tunnel geometry. This results in an

increase in resistance and a concomitant increase in detectable voltage. We have shown here that by bundling the axons into fascicles of approximately 10μm in diameter (Figure 12F), not only were we able to record the electrical activity from axonal bundles, but that these cultures elicited greater firing frequencies than the comparable two-dimensional conditions. While this result is striking, based on this set up of this experiment, it is not necessarily unexpected. The geometry of the cells coming in contact with the MEA electrodes may play a major role in the results. While the larger sized DRG somas may only allow for the recording of a few DRGNs at a time. In contrast, the small size of the axons allows for them to be packed in tightly together, possibly allowing for the recording of action potentials from more cells at once. It is also possible that more than one axon bundle could be being recorded on a single 30μm electrode. Alternatively, this high firing rate could be the result of ephaptic coupling. The organization of axons is shown in Figure 12D, where tight bundling of the axons together can be observed and the close approximation of each axon to another could lead to action potentials in one or more axons modulating the activity of others. This result has been previously postulated by studies using the two-dimensional microtunnel experiments (Dworak and Wheeler, 2009).

It is important to note that although we did our best to compare the Capgel™ culture with similar two-dimensional experiments, further experiments should be done to account for some of the differences that arise when culturing cells in this model. The DRG explants that are cultured on top of Capgel™ are in a different environment than the two-dimensional cultures. These explants are cultured on the gel directly instead of on the MEA surface and approximately 2mm above this surface. At this location, the cells are nearly being cultured at an air-liquid interface, which could provide a stressful environment to which the cell response may be noticed by the

MEA recording of higher levels of spontaneous activity. Although theoretically this method of culturing could be detrimental to cell health, we did not see any evidence of axonal degradation when analyzed by immunohistochemistry and many of these cells responded to capsaicin treatment, further suggesting their viability. Future experiments will focus on the comparison of this 3D nerve model with other 3D configurations to further prove that it is the bundling of axons, which has led to such a dramatic increase in DRG spontaneous activity.

The close approximation of the axonal bundles observed in this experiment bear a striking resemblance to the early developing peripheral nerves as the reach their targets. At this stage in development, the nerves are comprised of tightly bundled axons and glia, still lacking connective tissue between them (Jessen and Mirksy, 2005). This system lends itself well to the induction of myelination that was carried out in chapter 2 and it would be interesting to study the effects of this architectural difference on electrical activity. The myelination process involves the segregation of axons by Schwann cells into myelinated and unmyelinated axons and this separation event could abrogate any possible ephaptic coupling.

Action potential analysis showed multiple populations of action potentials coming from one electrode, suggesting multiple axons in an axon bundle are being recorded. Capsaicin was used in this experiment to stimulate DRG neurons to illustrate the heterogeneity of neuronal subtypes that make up the axonal bundles present. It has previously been shown that 1 μM of capsaicin is adequate to depolarize nociceptors in vitro (Newberry et al., 2016; Caterina et al., 2000; Wainger et al., 2015). Our analysis of waveforms, which showed an increase in frequency of more than one-fold in response to capsaicin treatment was around 64% (Figure 16B), which is similar to the reported percentage of nociceptor neurons in the DRG. Overall, this supports the

conclusion that we have recreated a functional 3D nerve model that resembles the in vivo nerve. This system can be applied to study pain and neural regeneration.

CHAPTER FOUR: CONCLUSIONS

In summary, we have developed a functional three-dimensional model of the peripheral nerve in-vitro. This model contains Schwann cell myelinated axons in a three-dimensional environment and for the first time, the formation of a rudimentary perineurium around a bundle of axons. Culturing DRGs through a capillary alginate gel (Capgel™) results in the development of nerve fascicles throughout the gel in multiple channels. These fascicles exhibit extracellular molecules observed in-vivo, including collagen IV deposited in a thick ring around the nerve fascicle. This ring is found to contain flat perineurial glia, which express Glut-1 and tight junctions (Claudin-1), which suggests the formation of perineurium in-vitro. This nerve model was further integrated with an MEA to take advantage of the bundled axons present in our model and the exclusion of neuronal soma.

The Capgel™ architecture presents us with unique factors that can be utilized for future experiments. We observed a separation of DRG cell bodies from axon bundles, which in effect has given us a three-dimensional Campenot chamber-like device. Just as in standard two-dimensional Campenot chambers, this Capgel™ culture maintains a separation of DRG cell bodies from the distal axonal bundles. This factor was utilized in our MEA experiments, which specifically allowed us to record electrical activity from axonal bundles and ensure that we were not recording from neuronal somas. Channel size of Capgel™ can be manipulated and in future experiments, it would be interesting to see if manipulating channel size could be used to manipulate fascicle size and complexity. In our experiments, the rudimentary perineurium structure that formed was comprised of perineurial glia only one to two cell layers thick. This result could be dependent on fascicle size or axon number, which is known to play a role in vivo

(Piña-Oviedo and Ortiz-Hidalgo, 2008). By using larger channel sizes in the gel, it would be interesting to see if larger diameter fascicles would form and if this would have any effect on the number of concentric layers formed in the perineurium-like structure.

In this model, axons extend from the DRG and into the microcapillary channels of Capgel™. These axons extend through the gel with associated glia, just as in early nerve development. Over the course of the experiment, Schwann cell segregation of axons and subsequent myelination occurs. Interestingly, early developing nerves lack ECM until they reach their target innervations (Jessen and Mirsky, 2005). Our results clearly show that both laminin and collagen IV are deposited in our in vitro generated nerve fascicles when analyzed at 35 DIV, further suggesting proof that these nerves are mimicking in vivo developmental processes. Based on this observation, this model can be used to study the early development of the peripheral nerve and look for factors such as ECM deposition and perineurium formation. Schwann cell derived Desert hedgehog (Dhh) is one of the factors necessary for perineurium development and normal nerve fasciculation in vivo (Parmantier et al., 1999), but little else is known about the process which forms the mature perineurium (Figure 18). This model could be used to explore this complex process.

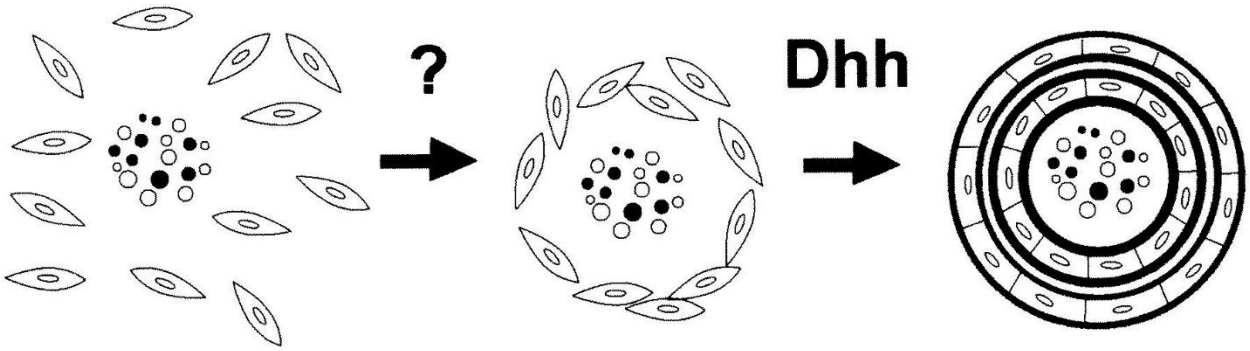

Figure 18 Perineurium development.

While the cells that give rise to motor nerve perineurium development have been elucidated (Kucenas et al., 2008) the cells that develop into the sensory nerve perineurium are currently being debated. Traditionally it was thought that perineurial glia differentiated from fibroblasts, arising from the mesoderm (Shantha and Bourne, 1968). In vitro experiments have suggested that fibroblasts when cultured with neurons and Schwann cells formed a perineurium like structure that ensheathed bundles of axons (Bunge et al., 1989). Evidence linking perineurial glial cells deriving from the neuroectoderm has recently been shown with Nkx2.2 cells from the CNS forming the perineurium (Clark et al., 2014). These experiments focused on the neuroectoderm lineage for motor nerve perineurium, but currently the origin of sensory nerve perineurial glia is unknown (Kucenas, 2015). The model described here can be used to study the origin of sensory nerve perineurium. We have shown the development of a rudimentary perineurium derived from an embryonic DRG explant inserted into Capgel™. The presence of mature Glut-1 positive glial cells, ensheathing nerve fascicles with collagen IV and tight junction marker (claudin-1) colocalization illustrate a structure which represents a developing

perineurium whose origin could be tracked using this model. Perineurial cells deriving from the embryonic DRG do suggest a neural crest lineage, possibly arising from SCPs and further experiments could be done to test this idea.

The three-dimensional nerve model generated here provides a platform to study nerve regeneration. The unique structure of the nerve lends itself for a variety of physical manipulations. For instance, the developed nerve structure generated here could be transected, just as peripheral nerves are in nerve injuries in vivo (Campbell et al., 2008) (Figure 19A). This would allow for the study of peripheral nerve regeneration as well as Wallerian degeneration. Wallerian degeneration is a process that happens after nerve injury where the nerve distal from the injury site degenerates (Figure 19B). This process has been largely studied and the following regeneration mechanism has major implications for nerve regeneration. Perineurial glia specifically, play a major role in early nerve regeneration and are among the first to bridge the injury site (Figure 19C). This allows for the recruitment, migration, and proliferation of Schwann cells from the proximal stump to the distal site and promotes regeneration (Figure 19D) and the reinnervation of their target sites (Figure 19E). Furthermore, in the model presented here the effects on the DRGN cell bodies and associated satellite glia could also be studied. In transected nerves signals are sent to the originating neuronal cell bodies and switch the axons and glia into a regenerative state. The structure of the Capgel™ generated nerves means that both sites could be studied at once and used to investigate reparative mechanisms. Work in our lab has been done in which satellite glial cells were isolated (George et al., 2018) and their involvement could be looked at with this model in terms of nerve injury.

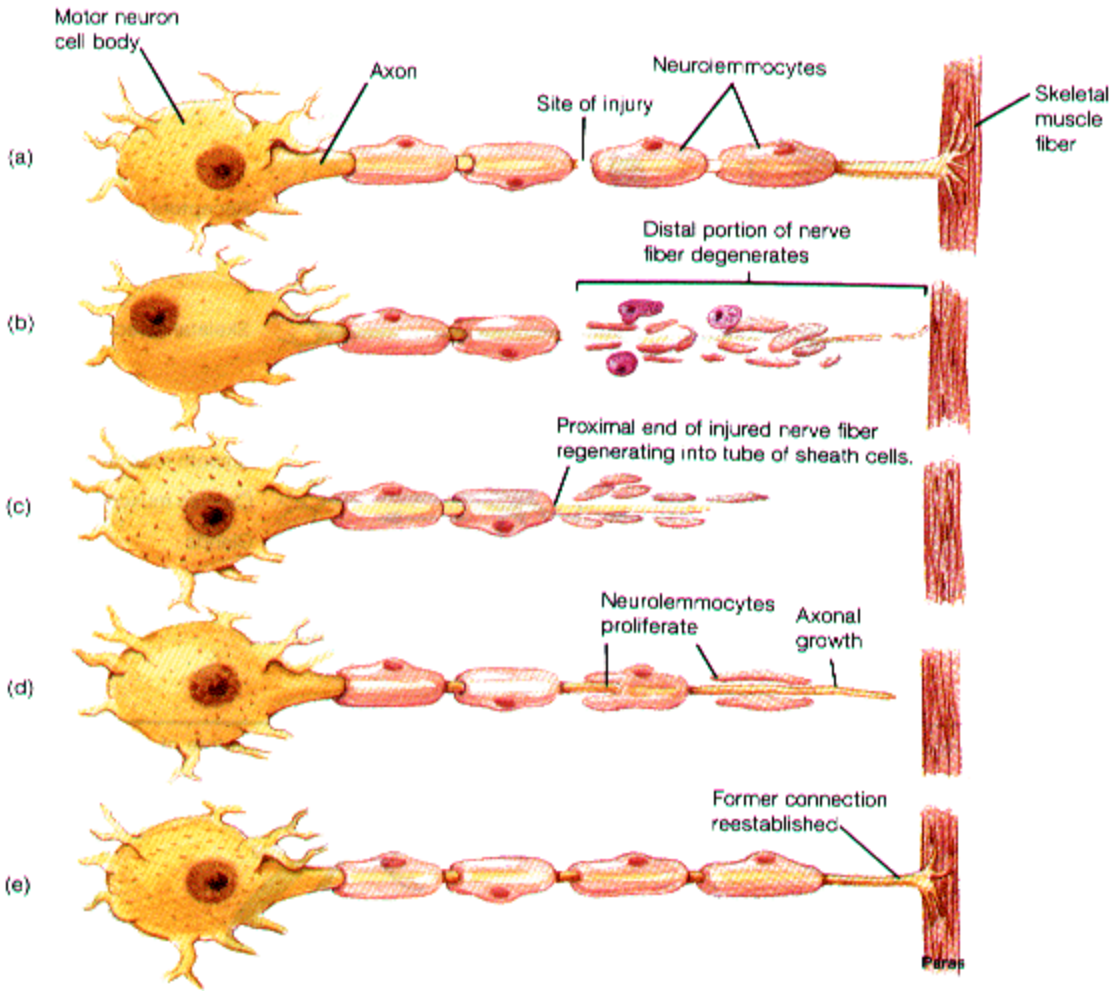

Figure 19 Wallerian degeneration and peripheral nerve regeneration

To generate a functional three-dimensional model of the peripheral nerve, our nerve model was integrated with a microelectrode array. This experiment required no further alteration of the MEA surface, illustrating the ease of use of our nerve model, compared to other models which require complicated preparation such as patterning of the MEA. With this Capgel™ culture, DRG cell bodies had low migratory distances through the gel capillaries ensuring that the spontaneous activity recorded was solely from neuronal axon bundles.

By analyzing action potential wave forms from the neuronal axons, we were able to discern multiple action potential wave forms from a single electrode. This suggests that we are recording from multiple axons in a single axon bundle. This was further tested by introducing the capsaicin, which is known to increase neuronal electrical activity of nociceptors. As expected, well wide mean firing rate increased when compared to control cultures. Interestingly, not all neurons had increased firing rates when analyzed. The DRG is made of a heterogeneous population of neurons including the capsaicin sensitive nociceptors and capsaicin insensitive neurons. This suggests that our neuronal axon bundles are heterogeneous in nature, which further mimics the in vivo peripheral nerve. This model has the potential to be used as a testbed for therapeutic development of factors involved in pain. The integration of our nerve model with the MEA supports a nerve-machine interface, which has applications for neuroprosthetics and pain modulation.

This study demonstrates the first in-vitro system developed with 3D nerve fascicle and perineurium formation highlighting its use for peripheral nerve research in-vitro. The more faithful representation of the in vivo nerve structure will likely result in the elucidation of complex mechanisms involved in nerve development, degeneration, and regeneration. This system can further be used to study Schwann cell-axon interactions in 3D as well as perineurial glia and perineurium formation and properties. In the future, this system will be used for clinically relevant studies for peripheral nerve regeneration and diseases of peripheral nerve glia.

A logical next step for this in vitro nerve model is to use human derived cells. Generating these nerve models using human cells will help reduce animal experimentation and improve drug development processes for clinical applications such as nerve regeneration. Previously, human

neural stem cells have formed Schwann cells and sensory neurons in vitro (Guo et al., 2013). Human DRGs have also been cultured on an MEA (Enright et al., 2016). The Capgel nerve model presented here could adapted to a human platform. The characterization of such structures would be insightful for future research into peripheral nerve diseases and regeneration.

LIST OF REFERENCES

Akert, K., Sandri, C., Weibel, E. R., Peper, K., & Moor, H. (1976). The fine structure of the perineural endothelium. *Cell Tissue Res, 165*(3), 281-295.

Anderson, W. A., Willenberg, A. R., Bosak, A. J., Willenberg, B. J., & Lambert, S. (2018). Use of a capillary alginate gel (Capgel) to study the three-dimensional development of sensory nerves reveals the formation of a rudimentary perineurium. *J Neurosci Methods*. doi:10.1016/j.jneumeth.2018.05.003

Braga Silva, J., Marchese, G. M., Cauduro, C. G., & Debiasi, M. (2017). Nerve conduits for treating peripheral nerve injuries: A systematic literature review. *Hand Surg Rehabil, 36*(2), 71-85. doi:10.1016/j.hansur.2016.10.212

Breslin, S., & O'Driscoll, L. (2013). Three-dimensional cell culture: the missing link in drug discovery. *Drug Discov Today, 18*(5-6), 240-249. doi:10.1016/j.drudis.2012.10.003

Brushart, T. M. (1991). Central course of digital axons within the median nerve of Macaca mulatta. *J Comp Neurol, 311*(2), 197-209. doi:10.1002/cne.903110203

Buitenweg, J. R., Rutten, W. L., & Marani, E. (2002). Modeled channel distributions explain extracellular recordings from cultured neurons sealed to microelectrodes. *IEEE Trans Biomed Eng, 49*(12 Pt 2), 1580-1590. doi:10.1109/TBME.2002.805555

Bunge, M. B., Wood, P. M., Tynan, L. B., Bates, M. L., & Sanes, J. R. (1989). Perineurium originates from fibroblasts: demonstration in vitro with a retroviral marker. *Science, 243*(4888), 229-231.

Bunge, M. B., Wood, P. M., Tynan, L. B., Bates, M. L., & Sanes, J. R. (1989). Perineurium originates from fibroblasts: demonstration in vitro with a retroviral marker. *Science, 243*(4888), 229-231.

Campenot, R. B. (1977). Local control of neurite development by nerve growth factor. *Proc Natl Acad Sci U S A, 74*(10), 4516-4519.

Campenot, R. B., Draker, D. D., & Senger, D. L. (1994). Evidence That Protein-Kinase-C Activities Involved in Regulating Neurite Growth Are Localized to Distal Neurites. *Journal of Neurochemistry, 63*(3), 868-878.

Caterina, M. J., Leffler, A., Malmberg, A. B., Martin, W. J., Trafton, J., Petersen-Zeitz, K. R., . . . Julius, D. (2000). Impaired nociception and pain sensation in mice lacking the capsaicin receptor. *Science, 288*(5464), 306-313. doi:DOI 10.1126/science.288.5464.306

Caterina, M. J., Schumacher, M. A., Tominaga, M., Rosen, T. A., Levine, J. D., & Julius, D. (1997). The capsaicin receptor: a heat-activated ion channel in the pain pathway. *Nature, 389*(6653), 816-824.

Chang, J. C., Brewer, G. J., & Wheeler, B. C. (2001). Modulation of neural network activity by patterning. *Biosens Bioelectron, 16*(7-8), 527-533.

Clark, J. K., O'Keefe, A., Mastracci, T. L., Sussel, L., Matise, M. P., & Kucenas, S. (2014). Mammalian Nkx2.2+ perineurial glia are essential for motor nerve development. *Dev Dyn, 243*(9), 1116-1129. doi:10.1002/dvdy.24158

Cravioto, H. (1965). Studies on the normal ultrastructure of peripheral nerve: axis cylinders, Schwann cells and myelin. *Bull Los Angeles Neurol Soc, 30*(4), 169-190.

Daly, W., Yao, L., Zeugolis, D., Windebank, A., & Pandit, A. (2012). A biomaterials approach to peripheral nerve regeneration: bridging the peripheral nerve gap and enhancing functional recovery. *J R Soc Interface, 9*(67), 202-221. doi:10.1098/rsif.2011.0438

Daud, M. F., Pawar, K. C., Claeyssens, F., Ryan, A. J., & Haycock, J. W. (2012). An aligned 3D neuronal-glial co-culture model for peripheral nerve studies. *Biomaterials, 33*(25), 5901-5913. doi:10.1016/j.biomaterials.2012.05.008

de Ruiter, G. C., Malessy, M. J., Yaszemski, M. J., Windebank, A. J., & Spinner, R. J. (2009). Designing ideal conduits for peripheral nerve repair. *Neurosurg Focus, 26*(2), E5. doi:10.3171/FOC.2009.26.2.E5

Della Rocca, D. G., Willenberg, B. J., Ferreira, L. F., Wate, P. S., Petersen, J. W., Handberg, E. M., . . . Pepine, C. J. (2012). A degradable, bioactive, gelatinized alginate hydrogel to improve stem cell/growth factor delivery and facilitate healing after myocardial infarction. *Med Hypotheses, 79*(5), 673-677. doi:10.1016/j.mehy.2012.08.006

Dworak, B. J., & Wheeler, B. C. (2009). Novel MEA platform with PDMS microtunnels enables the detection of action potential propagation from isolated axons in culture. *Lab Chip, 9*(3), 404-410. doi:10.1039/b806689b

Egert, U., Knott, T., Schwarz, C., Nawrot, M., Brandt, A., Rotter, S., & Diesmann, M. (2002). MEA-Tools: an open source toolbox for the analysis of multi-electrode data with MATLAB. *J Neurosci Methods, 117*(1), 33-42.

Faroni, A., Mobasseri, S. A., Kingham, P. J., & Reid, A. J. (2015). Peripheral nerve regeneration: experimental strategies and future perspectives. *Adv Drug Deliv Rev, 82-83*, 160-167. doi:10.1016/j.addr.2014.11.010

Fogt, F., Capodieci, P., & Loda, M. (1995). *Assessment of perineural invasion by GLUT-1 immunohistochemistry* (Vol. 3).

Garratt, A. N., Britsch, S., & Birchmeier, C. (2000). Neuregulin, a factor with many functions in the life of a schwann cell. *Bioessays, 22*(11), 987-996. doi:10.1002/1521-1878(200011)22:11<987::AID-BIES5>3.0.CO;2-5

Gatto, C. L., Walker, B. J., & Lambert, S. (2003). Local ERM activation and dynamic growth cones at Schwann cell tips implicated in efficient formation of nodes of Ranvier. *J Cell Biol, 162*(3), 489-498. doi:10.1083/jcb.200303039

George, D., Ahrens, P., & Lambert, S. (2018). Satellite glial cells represent a population of developmentally arrested Schwann cells. *Glia, 66*(7), 1496-1506. doi:10.1002/glia.23320

Grinsell, D., & Keating, C. P. (2014). Peripheral nerve reconstruction after injury: a review of clinical and experimental therapies. *Biomed Res Int, 2014*, 698256. doi:10.1155/2014/698256

Hanani, M., Huang, T. Y., Cherkas, P. S., Ledda, M., & Pannese, E. (2002). Glial cell plasticity in sensory ganglia induced by nerve damage. *Neuroscience, 114*(2), 279-283. doi:Pii S0306-4522(02)00279-8

Doi 10.1016/S0306-4522(02)00279-8

Heinricher, M. M., Cheng, Z. F., & Fields, H. L. (1987). Evidence for 2 Classes of Nociceptive Modulating Neurons in the Periaqueductal Gray. *Journal of Neuroscience, 7*(1), 271-278.

Huval, R. M., Miller, O. H., Curley, J. L., Fan, Y., Hall, B. J., & Moore, M. J. (2015). Microengineered peripheral nerve-on-a-chip for preclinical physiological testing. *Lab Chip, 15*(10), 2221-2232. doi:10.1039/c4lc01513d

Jessen, K. R., & Mirsky, R. (1999). Schwann cells and their precursors emerge as major regulators of nerve development. *Trends Neurosci, 22*(9), 402-410.

Jessen, K. R., & Mirsky, R. (2005). The origin and development of glial cells in peripheral nerves. *Nat Rev Neurosci, 6*(9), 671-682. doi:10.1038/nrn1746

Jessen, K. R., Mirsky, R., & Lloyd, A. C. (2015). Schwann Cells: Development and Role in Nerve Repair. *Cold Spring Harb Perspect Biol, 7*(7), a020487. doi:10.1101/cshperspect.a020487

Johnstone, A. F., Gross, G. W., Weiss, D. G., Schroeder, O. H., Gramowski, A., & Shafer, T. J. (2010). Microelectrode arrays: a physiologically based neurotoxicity testing platform for the 21st century. *Neurotoxicology, 31*(4), 331-350. doi:10.1016/j.neuro.2010.04.001

Joseph, N. M., Mukouyama, Y. S., Mosher, J. T., Jaegle, M., Crone, S. A., Dormand, E. L., . . . Morrison, S. J. (2004). Neural crest stem cells undergo multilineage differentiation in

developing peripheral nerves to generate endoneurial fibroblasts in addition to Schwann cells. *Development, 131*(22), 5599-5612. doi:10.1242/dev.01429

Kim, J. H., Kim, J. H., Park, J. A., Lee, S. W., Kim, W. J., Yu, Y. S., & Kim, K. W. (2006). Blood-neural barrier: intercellular communication at glio-vascular interface. *J Biochem Mol Biol, 39*(4), 339-345.

Kucenas, S. (2015). Perineurial glia. *Cold Spring Harb Perspect Biol, 7*(6). doi:10.1101/cshperspect.a020511

Kucenas, S., Snell, H., & Appel, B. (2008). nkx2.2a promotes specification and differentiation of a myelinating subset of oligodendrocyte lineage cells in zebrafish. *Neuron Glia Biol, 4*(2), 71-81. doi:10.1017/S1740925X09990123

Lewandowska, M. K., Bakkum, D. J., Rompani, S. B., & Hierlemann, A. (2015). Recording large extracellular spikes in microchannels along many axonal sites from individual neurons. *PLoS One, 10*(3), e0118514. doi:10.1371/journal.pone.0118514

Lundborg, G. (2003). Richard P. Bunge memorial lecture. Nerve injury and repair--a challenge to the plastic brain. *J Peripher Nerv Syst, 8*(4), 209-226.

Luscher, C., Streit, J., Quadroni, R., & Luscher, H. R. (1994). Action potential propagation through embryonic dorsal root ganglion cells in culture. I. Influence of the cell morphology on propagation properties. *J Neurophysiol, 72*(2), 622-633. doi:10.1152/jn.1994.72.2.622

Marmigere, F., & Ernfors, P. (2007). Specification and connectivity of neuronal subtypes in the sensory lineage. *Nature Reviews Neuroscience, 8*(2), 114-127. doi:10.1038/nrn2057

Montano, J. A., Perez-Pinera, P., Garcia-Suarez, O., Cobo, J., & Vega, J. A. (2010). Development and Neuronal Dependence of Cutaneous Sensory Nerve Formations: Lessons From Neurotrophins. *Microscopy Research and Technique, 73*(5), 513-529. doi:10.1002/jemt.20790

Moraes, E. R., Kushmerick, C., & Naves, L. A. (2014). Characteristics of dorsal root ganglia neurons sensitive to Substance P. *Mol Pain, 10*, 73. doi:10.1186/1744-8069-10-73

Narula, U., Ruiz, A., McQuaide, M., DeMarse, T. B., Wheeler, B. C., & Brewer, G. J. (2017). Narrow microtunnel technology for the isolation and precise identification of axonal communication among distinct hippocampal subregion networks. *PLoS One, 12*(5), e0176868. doi:10.1371/journal.pone.0176868

Newberry, K., Wang, S., Hoque, N., Kiss, L., Ahlijanian, M. K., Herrington, J., & Graef, J. D. (2016). Development of a spontaneously active dorsal root ganglia assay using multiwell multielectrode arrays. *J Neurophysiol, 115*(6), 3217-3228. doi:10.1152/jn.01122.2015

Obien, M. E., Deligkaris, K., Bullmann, T., Bakkum, D. J., & Frey, U. (2014). Revealing neuronal function through microelectrode array recordings. *Front Neurosci, 8*, 423. doi:10.3389/fnins.2014.00423

Ortiz-Hidalgo, C., & Weller, R. O. (1997). *Peripheral nervous system. In Sternberg, SS Histology for Pathologists* (2nd ed. ed.). Philadelphia: Lippincott-Raven.

Parmantier, E., Lynn, B., Lawson, D., Turmaine, M., Namini, S. S., Chakrabarti, L., . . . Mirsky, R. (1999). Schwann cell-derived Desert hedgehog controls the development of peripheral nerve sheaths. *Neuron, 23*(4), 713-724.

Pawar, K., Mueller, R., Caioni, M., Prang, P., Bogdahn, U., Kunz, W., & Weidner, N. (2011). Increasing capillary diameter and the incorporation of gelatin enhance axon outgrowth in alginate-based anisotropic hydrogels. *Acta Biomater, 7*(7), 2826-2834. doi:10.1016/j.actbio.2011.04.006

Pina-Oviedo, S., & Ortiz-Hidalgo, C. (2008). The normal and neoplastic perineurium: a review. *Adv Anat Pathol, 15*(3), 147-164. doi:10.1097/PAP.0b013e31816f8519

Prang, P., Muller, R., Eljaouhari, A., Heckmann, K., Kunz, W., Weber, T., . . . Weidner, N. (2006). The promotion of oriented axonal regrowth in the injured spinal cord by alginate-based anisotropic capillary hydrogels. *Biomaterials, 27*(19), 3560-3569. doi:10.1016/j.biomaterials.2006.01.053

Schmalbruch, H. (1986). Fiber composition of the rat sciatic nerve. *Anat Rec, 215*(1), 71-81. doi:10.1002/ar.1092150111

Scott, S. A. (1992). *Sensory neurons : diversity, development, and plasticity*. New York: Oxford University Press.

Shantha, T. R., Golarz, M. N., & Bourne, G. H. (1968). Histological and histochemical observations on the capsule of the muscle spindle in normal and denervated muscle. *Acta Anat (Basel), 69*(4), 632-646.

Stenger, D. A., Hickman, J. J., Bateman, K. E., Ravenscroft, M. S., Ma, W., Pancrazio, J. J., . . . Cotman, C. W. (1998). Microlithographic determination of axonal/dendritic polarity in cultured hippocampal neurons. *J Neurosci Methods, 82*(2), 167-173.

Stewart, J. D. (2003). Peripheral nerve fascicles: anatomy and clinical relevance. *Muscle Nerve, 28*(5), 525-541. doi:10.1002/mus.10454

Taylor, C. A., Braza, D., Rice, J. B., & Dillingham, T. (2008). The incidence of peripheral nerve injury in extremity trauma. *Am J Phys Med Rehabil, 87*(5), 381-385. doi:10.1097/PHM.0b013e31815e6370

Tominaga, M., Caterina, M. J., Malmberg, A. B., Rosen, T. A., Gilbert, H., Skinner, K., . . . Julius, D. (1998). The cloned capsaicin receptor integrates multiple pain-producing stimuli. *Neuron, 21*(3), 531-543. doi:Doi 10.1016/S0896-6273(00)80564-4

Trotter, J., Crang, A. J., Schachner, M., & Blakemore, W. F. (1993). Lines of glial precursor cells immortalised with a temperature-sensitive oncogene give rise to astrocytes and oligodendrocytes following transplantation into demyelinated lesions in the central nervous system. *Glia, 9*(1), 25-40. doi:10.1002/glia.440090105

van Pelt, J., Wolters, P. S., Corner, M. A., Rutten, W. L., & Ramakers, G. J. (2004). Long-term characterization of firing dynamics of spontaneous bursts in cultured neural networks. *IEEE Trans Biomed Eng, 51*(11), 2051-2062. doi:10.1109/TBME.2004.827936

Wainger, B. J., Buttermore, E. D., Oliveira, J. T., Mellin, C., Lee, S., Saber, W. A., . . . Woolf, C. J. (2015). Modeling pain in vitro using nociceptor neurons reprogrammed from fibroblasts. *Nature Neuroscience, 18*(1), 17-+. doi:10.1038/nn.3886

Wanner, I. B., Guerra, N. K., Mahoney, J., Kumar, A., Wood, P. M., Mirsky, R., & Jessen, K. R. (2006). Role of N-cadherin in Schwann cell precursors of growing nerves. *Glia, 54*(5), 439-459. doi:10.1002/glia.20390

Willenberg, B. J., Hamazaki, T., Meng, F. W., Terada, N., & Batich, C. (2006). Self-assembled copper-capillary alginate gel scaffolds with oligochitosan support embryonic stem cell growth. *J Biomed Mater Res A, 79*(2), 440-450. doi:10.1002/jbm.a.30942

Willenberg, B. J., Zheng, T., Meng, F. W., Meneses, J. C., Rossignol, C., Batich, C. D., . . . Weiss, M. D. (2011). Gelatinized copper-capillary alginate gel functions as an injectable tissue scaffolding system for stem cell transplants. *J Biomater Sci Polym Ed, 22*(12), 1621-1637. doi:10.1163/092050610X519453

Wiltschko, A. B., Gage, G. J., & Berke, J. D. (2008). Wavelet filtering before spike detection preserves waveform shape and enhances single-unit discrimination. *J Neurosci Methods, 173*(1), 34-40. doi:10.1016/j.jneumeth.2008.05.016

Windebank, A. J., Wood, P., Bunge, R. P., & Dyck, P. J. (1985). Myelination determines the caliber of dorsal root ganglion neurons in culture. *J Neurosci, 5*(6), 1563-1569.

Wood, F., Black, M. J., Vargas-Irwin, C., Fellows, M., & Donoghue, J. P. (2004). On the variability of manual spike sorting. *IEEE Trans Biomed Eng, 51*(6), 912-918. doi:10.1109/TBME.2004.826677

Wood, P., Moya, F., Eldridge, C., Owens, G., Ranscht, B., Schachner, M., . . . Bunge, R. (1990). Studies of the initiation of myelination by Schwann cells. *Ann N Y Acad Sci, 605*, 1-14.

Wood, P. M., & Bunge, R. P. (1975). Evidence That Sensory Axons Are Mitogenic for Schwann-Cells. *Nature, 256*(5519), 662-664. doi:DOI 10.1038/256662a0

Xiao, J., Wong, A. W., Willingham, M. M., Kaasinen, S. K., Hendry, I. A., Howitt, J., . . . Murray, S. S. (2009). BDNF exerts contrasting effects on peripheral myelination of NGF-dependent and BDNF-dependent DRG neurons. *J Neurosci, 29*(13), 4016-4022. doi:10.1523/JNEUROSCI.3811-08.2009